THE DEVELOPMENT OF THE BLENDED FIBROIN/HEMP CBD DRESSING FOR THE TREATMENT OF CHRONIC WOUND

THAMONPHAT KLINSANG

A Thesis Submitted to the Graduate School of Naresuan University
in Partial Fulfillment of the Requirements
for the Master of Science in Pharmacology and Biomolecular Sciences
2022

มหาวิทยาลัยนเรศวร

THE DEVELOPMENT OF THE BLENDED FIBROIN/HEMP CBD DRESSING FOR THE TREATMENT OF CHRONIC WOUND

THAMONPHAT KLINSANG

A Thesis Submitted to the Graduate School of Naresuan University
in Partial Fulfillment of the Requirements
for the Master of Science in Pharmacology and Biomolecular Sciences
2022

Thesis entitled "The development of the blended fibroin/hemp CBD dressing for the treatment of chronic wound"

By Thamonphat Klinsang

has been approved by the Graduate School as partial fulfillment of the requirements for the Master of Science in Pharmacology and Biomolecular Sciences of Naresuan University

Oral Defense Committee

..... Chair
(Nontaphat Leerach, Ph.D.)

..... Advisor
(Professor Jarupa Viyoch, Ph.D.)

..... Co Advisor
(Assistant Professor Pensri Charoensit, Ph.D.)

..... Co Advisor
(Associate Professor Sukunya Ross, Ph.D.)

..... Internal Examiner
(Associate Professor Aurasorn Saraphanchotiwitthaya, Ph.D.)

Approved

.....
(Associate Professor Krongkarn Chootip, Ph.D.)
Dean of the Graduate School

Title	THE DEVELOPMENT OF THE BLENDED FIBROIN/HEMP CBD DRESSING FOR THE TREATMENT OF CHRONIC WOUND
Author	Thamonphat Klinsang
Advisor	Professor Jarupa Viyoch, Ph.D.
Co-Advisor	Assistant Professor Pensri Charoensit, Ph.D. Associate Professor Sukunya Ross, Ph.D.
Academic Paper	M.S. Thesis in Pharmacology and Biomolecular Sciences, Naresuan University, 2022
Keywords	Hemp Cannabidiol Fibroin Wound dressing Delayed wound healing Chronic wound

ABSTRACT

A delayed or chronic wound in patients with diabetes is a common and significant problem in Thailand. An appropriate wound dressing can promote chronic wound healing, leading to a better quality of life for patients with diabetes. The objective of this study was to develop a blended fibroin/CBD complex dressing to treat chronic wounds. Fibroin was extracted from *Bombyx morí* cocoons, with a protein content was 96.34 ± 0.14% by weight. The fibroin comprised at least two protein groups, including heavy chains and light chains, ranging from 25-325 kDa. The chemical identity of the extracted protein was confirmed using FTIR spectroscopy. The preparation of cannabidiol as a cannabidiol/ 2-hydroxypropyl-beta-cyclodextrin inclusion complex (CBD complex) enhanced cannabidiol solubility. The blended fibroin/CBD complex dressing preparation contained 6.2 mg of cannabidiol per sheet. Cytotoxicity test showed that the blended fibroin/CBD complex film was not toxic to Normal Human Dermal Fibroblast cells (NHDF). In addition, cell cycle analysis using flow cytometry revealed that the blended fibroin/CBD complex dressing promoted DNA replication. After being treated with the blended fibroin/CBD complex dressing, the percentage of G2/M phase in cell cycle was higher than those treated with the fibroin dressing without CBD. Therefore, the blended fibroin/CBD complex film elevated cell proliferation. In addition, in a diabetic rat model, the chronic wound treated with the blended fibroin/CBD complex dressing

dried faster and was more compact after seven days of therapy than the control groups. These results indicated that cannabidiol from hemp can be incorporated into a fibroin dressing and applied to chronic wounds to achieve successful outcomes with no toxicity indicated.

ACKNOWLEDGEMENTS

The researcher would like to express much appreciation to Professor Jarupa Viyoch and co-advisers Assistant Professor Pensri Charoensit and Associate Professor Sukunya Ross for their time, effort, and understanding in assisting me with my studies. Furthermore, the Agricultural Research and Development Agency (ARDA) for the grant provided for this research (Grant Number CRP6105022940). Furthermore, we would like to extend our gratitude to the Center of Excellence for Innovation in Chemistry (PERCH-CIC), the Office of the Higher Education Commission, the Global and Frontier Research University (Grant Number R2566C052, Naresuan University), and also to the Faculty of Pharmaceutical Sciences, Naresuan University for the exceptional support and the well-resourced facilities provided, which help make this study accomplished its goals. Our thanks to Mr. Roy I. Morien and Mr. Reggie Dalman Hinoguin of the Naresuan University Graduate School for their editing of the grammar, syntax, and general English expression in this thesis.

And I would like to thank Dr. Kunlathida Luangpraditkun, Dr. Preeyawass Phimnuan, Dr. Poonyawat Kusonwattana, Dr. Nattakit Yuduang, Thanawut Warakichpoonphol for their technical support during my research. I want to offer my appreciation to everyone at the JV lab and friends in COSNAT. My experience at NU has been highly beneficial because of their kindness and encouragement. Finally, I want to thank my parents and friends. It was only possible for me to complete my education with their constant support throughout the years.

Thamonphat Klinsang

TABLE OF CONTENTS

Page

ABSTRACT C

ACKNOWLEDGEMENTS ..... E

TABLE OF CONTENTS ..... F

LIST OF TABLES I

LIST OF FIGURES ..... J

CHAPTER I 1

INTRODUCTION 1

Background and Significance of the Study 1

Purposes of the study 2

Scope of the study 2

Keywords 3

CHAPTER II 4

LITERATURE REVIEW 4

Wound healing 4

Chronic wounds 6

Wound management 7

Silk fibroin 8

Cannabidiol (CBD) 11

Pharmacology and biochemistry of CBD 12

Mechanism of Action 12

CHAPTER III 14

METHODOLOGY 14

Chemical and materials 14

Instruments 15

Plant collection 16

Silkworm yellow cocoons 16
Cannabidiol (CBD)....16
Preparation of silk fibroin extracts 16
Characterization of isolated fibroin extract 17
Protein determination of the isolated fibroin....17
Determination of the molecular weight pattern....17
Fourier transform infrared spectroscopy (FTIR) analysis of the isolated fibroin 17
Cannabidiol with 2-Hydroxypropyl-β-cyclodextrin (HP-β-CD) inclusion complexes (CBD complex) 17
Preparation of CBD with 2-hydroxypropyl-β-cyclodextrin complex 17
Quantification of cannabidiol in the CBD complex....18
FTIR analysis of CBD complex 18
Field emission scanning electron microscopy (FE-SEM) analysis....18
X-ray diffraction (XRD) 19
Development of fibroin and CBD complex film (developed film) 19
Preparation of fibroin and CBD complex film....19
Sterilization of the developed film 19
Evaluation of the physicochemical properties developed film 19
FTIR analysis 20
Field emission scanning electron microscopy (FE-SEM) analysis....20
Mechanical properties 20
The effect of the developed film on the biological functions of Normal Human Dermal Fibroblasts (NHDF) cell 20
Cell culture 20
Cytotoxicity test 21
cell cycle analysis....21
Wound Healing Scratch Assay....21
Expression of growth factors by immunofluorescence 22
The effect of the developed film on streptozotocin-induced diabetic rat models....23

Experiment animals....23
Streptozotocin-induced diabetic rats....23
Wound creation....23
Treatment....23
Wound evaluation....24
Hematoxylin and Eosin Stain (H&E)....24
Hydroxyproline assay....24
Statistical analysis....25
CHAPTER IV....26
RESULT AND DISCUSSION....26
Characteristics of the isolated fibroin extract....26
Physico-chemical characteristics and qualification of CBD complex....27
Characteristics of the blended fibroin/CBD complex film....31
Physico-chemical characteristics of blended fibroin/CBD complex film....31
Biological activities of blended fibroin/CBD complex film....35
in vitro study....35
Cytocompatibility....35
Cell migration....36
Cell cycle....37
VEGF by immunoassay....40
in vivo study....41
Wound evaluation....41
Hematoxylin and Eosin (H&E) staining....42
Hydroxyproline assay....43
CHAPTER V....45
CONCLUSIONS....45
REFERENCES....47
BIOGRAPHY....53

LIST OF TABLES

Page

Table 1 Structure of silk fiber 9

LIST OF FIGURES

Page

Figure 1 International Diabetes Federation (IDF), in 2021 6

Figure 2 Schematic diagram of the silk structure. (A) heavy chain (i.e., N-terminus, β-sheets, Amorphous and C-terminus) and a light chain which is linked via disulphide bonds. (B) silkworm thread, fibril overall structure and silk fibroin polypeptide chains 10

Figure 3 Chemical structure of cannabidiol (CBD).....12

Figure 4 Physical characteristic (A) molecular weight patterns (B) and IR spectrum (C) of isolated fibroin extract 27

Figure 5 Physical appearance (A), HPLC of the chromatogram (B), FT-IR spectra (C), Field emission scanning electron microscopy (FE-SEM) (D), and X-ray diffractometer (XRD) (E) of CBD, HP-β-CD, and CBD complex 30

Figure 6 Physical appearance of developed film (A); FT-IR spectra of fibroin, CBD complex, and developed film (B); XRD patterns of fibroin, CBD complex, and developed film (C), tensile strength and % elongation at break of fibroin, and developed film (D), HPLC of the CBD content in developed film (E) 33

Figure 7 Field emission scanning electron microscopy (FE-SEM) images of developed film (A: surface; C: tensile fracture surface) and fibroin film (B: surface; D: tensile fracture surface).....34

Figure 8 Percentage of cell viability of NHDF cells treated with fibroin film and developed film for 24 h (A). Data are expressed as percent of control group (untreated cells), and each column represents mean ± S.D in triplicate (n = 3); ***p<0.001. Cell morphology of NHDF treated with control group (untreated cell), fibroin film, and developed film at magnification of 20x (B) 36

Figure 9 Cell migration of NHDF cells treated with the developed film at 12, 24, 36 and 48 h as compared to control group (untreated cells) at magnification of 10x.....37

Figure 10 Cell cycle phases of NHDF cells treated with fibroin and developed film for 24 h compared to the control group (untreated cells). This figure shows the examples of cell cycle distribution in dot plots, histogram profiles (A) and percent of total cell (B), and each column represents mean ± S.D. in triplicate (n = 3); ***p<0.001 39

Figure 11 Immunofluorescence for VEGF expression of control group (untreated NHDF cells), fibroin and developed film at magnification of 20x.....41

Figure 12 Photographs of wound contraction in the control group (non-treated wound), fibroin film and developed film in both of non-diabetic and diabetic rats at days 0 and 7 42

Figure 13 Histological assessment of wound healing by hematoxylin and eosin (H&E) staining. control groups (non-created wound) (A, D); fibroin film (B, E); developed film (C, F). Scale bar 100 μm.....43

Figure 14 The determination of hydroxyproline secretion of the control group (non-treated wound), fibroin film and developed film in non-diabetic-induced and diabetic-induced rats for 7 days. Data are expressed as hydroxyproline content (μg/g tissue), and each column represents mean ± S.D. in triplicate (n=3); *** p<0.001.....44

CHAPTER I

INTRODUCTION

Background and Significance of the Study

The incidence of chronic ulcers among people with diabetes mellitus becomes a significant issue in Thailand. According to the International Diabetes Federation (IDF) reported in 2021, 537 million diabetes patients were reported worldwide suffering from chronic wounds which seriously affected their daily life. This disease was commonly found in older people with poor glycemic control and high blood pressure. Chronic ulcers in diabetic patients require various procedures, such as maintaining blood sugar levels, treating antibiotics, and using wound care. Among these wound films is the most convenient and accessible medical strategy. However, the therapeutic effects of these wound film products remain elusive, and these are inexpensive. Using natural substances readily available locally has been shown as being highly efficacious in the treatment. Fibroin from silk cocoon and cannabidiol (CBD) from hemp, have been used for developing wound films that contain non-organic solvents, have no toxic emissions, and are developed with inexpensive processes.

Most wound films on the market today are synthetic polymers with qualities that encourage quicker wound healing and the capacity to absorb liquids released from chronic wounds. For example, Kerraboot® products, prepared from polyacrylate derivatives, offer good liquid absorbency characteristics. In addition to producing growth factors that regulate skin tissue formation and keep the wound area moist, these characteristics lead to tissue replacement. Additionally, natural polymer products like Promogran®, made from collagen combined with oxidized cellulose, have been shown to prevent the action of matrix metalloproteinase which is an enzyme that breaks down connective tissue. As a result, collagen, which is generated in lower amounts in the skin of diabetes patients, makes it more difficult for wounds to heal. Hyaluronic acid-based wound films gradually release hyaluronic acid, allowing skin cells, such as keratinocytes, to relocate to the wound and speed up healing. However, these products are expensive because they need to be imported; for

example, Kerraboot® costs around 1,250 baht per set, and Promogran® costs approximately 650 baht per sheet (size 4.34 square inches). These products must be changed every 3-5 days resulting in higher expenses. Also, the clinical efficacy of these products is not well indicated.

Silk fibroin is a biocompatible and biodegradable biomaterial which acts on several signaling pathways stimulating cell proliferation and migration, promoting proangiogenic activity, and allowing quicker skin wound healing. Additionally, silk fibroin-based films provide a base for additional substances that stimulate tissue regeneration and reduce inflammation (Mazurek, 2022). Cannabidiol, or CBD, is an essential hemp constituent which acts as an anti-inflammatory, pain relief, and is an antioxidant with no psychoactive effects. CBD is interesting for treating inflammation-related disorders and symptoms, such as poor healing in diabetic ulcers. As a result, we have proposed the development of restorative materials in the form of films for clinical use by combining fibroin from silk from silkworm cocoons and cannabidiol from hemp that has been isolated and confirmed to be pure. The objective is to create a product containing essential substances that are effective in wound healing and reducing inflammation. As well as developing a wound film made without organic solvents, that manifests no hazardous emissions, the low cost of production is also an objective.

Purposes of the study

1. To develop blended fibroin film incorporating cannabidiol from hem
2. To evaluate the physicochemical properties of the developed fi
3. To investigate the effect of the developed film on the biological activities of human dermal fibroblasts
4. To determine the efficacy of the developed film for wound healing in streptozotocin-induced diabetic rat models.

Scope of the study

This study focuses on developing a wound film product from silk fibroin protein incorporating cannabidiol (CBD) from hemp. In addition, silk fibroin protein extract was characterized by a DC protein assay kit to identify the total level of protein.

To determine the molecular weight of fibroin protein was qualitatively analyzed by sodium dodecyl sulfate-polyacrylamide gel electrophoresis SDS-PAGE method and the chemical structure was characterized by the Fourier transform infrared (FTIR) spectroscopy technique.

Cannabidiol complexing with 2-hydroxy-beta-cyclodextrin was prepared by the inclusion complexes method. Characterization of CBD/2HPβCD inclusion complexes by HPLC analysis, FT-IR analysis, and FESEM analysis (Li et al., 2021).

The biological properties of the product were evaluated for its efficacy on the human fibroblast, the viability of which was examined using XTT Viability Cytotoxicity Kit. The cell proliferation was evaluated using a Cell Cycle assay. Vascular endothelial growth factor (VEGF) is a substance that helps encourage the growth of new blood vessels. The amount of VEGF expression was analyzed (Su et al., 2019).

This is an *in vivo* study and the procedures for the study have been approved by the Institutional Animal Ethics Committee (Registration No. NU- AE630714). The efficacy of the biological properties of the product was evaluated on Sprague-Dawley rats (male, 5-6 weeks). A ruler was used to measure the scale of the wound size and for area calculation. The re-epithelialization process was determined by hematoxylin and eosin staining, and hydroxyproline assays were measured to assess collagen levels. The product was studied for its physical and chemical stability (Cheng et al., 2018).

Keywords Wound healing, Chronic wound, Wound film, Fibroin protein, Silk cocoon, cannabidiol, hemp.

CHAPTER II

LITERATURE REVIEW

Wound healing

Wound healing in the skin is a complicated process that comprises four overlapping phases: blood stoppage (hemostasis), inflammation, cell proliferation, and remodeling. Each of these can be differentiated based on the types of a cell migrating into the wound area, in which specific cells such as keratinocytes, fibroblasts, and other cells in the skin's dermis communicate chemical signals to promote wound healing (Raghow, 1994).

Phase I: Hemostasis; Hemostasis is the process that causes a blood vessel to stop bleeding. The coagulation cascades are then initiated by clotting factors from the wounded skin (extrinsic system), and exposed collagen activates thrombocytes for aggregation (intrinsic system). Simultaneously, the wounded arteries undergo a 5- 10-minute vasoconstriction induced by platelets to decrease blood loss and replace the tissue gap with a blood clot composed of cytokines and growth factors. Certain growth factors, in combination with the fibrin molecules, fibronectin, vitronectin, and thrombospondins, produce a provisional matrix, which provides a scaffold structure for the migration of the leukocytes, keratinocytes, fibroblasts, and endothelial cells. (Martin, 1997)

Phase II: Inflammation; The inflammatory phase of wound healing starts immediately after hemostasis is achieved, with the primary objective of clearing pathogens and foreign material from the wound and containing the damage to a localized area. Vasodilation enhances vascular permeability, allowing neutrophils and monocytes to localize to the wound site. A complicated interaction of cytokines regulates this phase, which results in monocyte differentiation to macrophages. (Wynn & Barron, 2010)

Neutrophils produce mediators such as TNF-α, IL-1, and IL-6, which enhance the inflammatory response and promote VEGF and IL-8 for an effective repair response. Furthermore, they begin debridement by releasing active antibacterial compounds and proteinases (Eming et al., 2007). Approximately three days after injury, macrophages reach the area of damage and contribute to the continuing process by phagocytosing

pathogens and cell debris (Tziotzios et al., 2012). Growth factors chemokines and cytokines are also secreted. Apart from contributing to wound healing, these molecules help to maintain the healing process by activating the next phase of wound healing (proliferative phase) (Gurtner et al., 2008). The inflammatory response to injury is important for releasing growth factor and cytokine signals that control cell and tissue mobility.

Macrophages provide various functions, including host defense, inflammation promotion and resolution, apoptotic cell elimination, and cell proliferation and tissue regeneration following injury (Koh & DiPietro, 2011). Aside from their immunological functions as antigen-presenting cells and phagocytes during wound repair, macrophages are known to play an essential role in wound healing by the synthesis of numerous potent growth factors such as TGF- β, basic FGF, PDGF, and VEGF, which promote cell proliferation and synthesis of the extracellular matrix (ECM) molecules by resident skin cells (DiPietro & Polverini, 1993).

Phase III: Proliferation; The main goal of the healing process during the proliferation phase is to cover the wound area, produce granulation tissue, and restore the vascular network. Therefore, due to the migration of local fibroblasts along the fibrin network and the start of re-epithelialization from the wound site, capillary sprouting activates neovascularization and angiogenesis (Bauer et al., 2005; Robson et al., 2001). The synthesis of collagen, fibronectin, and other basic substances are required for wound healing by fibroblasts under the control of regulating cytokines such as IFN-γ and TGF-β represent the basis for the new matrix of connective tissue, supporting the closure of tissue gaps and the restoration of the mechanical strength of the wound. Subsequently, collagen production increases throughout the wound, whereas fibroblast proliferation gradually decreases, adjusting the balance between ECM synthesis and breakdown (Madden & Peacock, 1971).

Phase IV: Remodeling; Remodeling is the final stage of wound healing and occurs from day 21 to a year following injury. The production of granulation tissue is stopped by cell apoptosis. As a result, a developed wound is both avascular and acellular. (Greenhalgh, 1998) Specific changes occur to the components of the ECM during wound development. Collagen III is created during the proliferative phase and is replaced by collagen I, which is more robust. Collagen I is arranged in short parallel bundles which

are very different from the basket-weave collagen found in the healthy dermis. (Gurtner & Evans, 2000) Subsequently, myofibroblasts produce wound contraction through their numerous collagen linkages and contribute to the decrease of the surface of the growing scar (Tziotzios et al., 2012). Furthermore, angiogenic activities drop, wound blood flow decreases, and acute wound metabolic activity slows and finally stops.

Chronic wounds

Due to an increased occurrence of chronic diseases such as obesity and diabetes resulting from an unhealthy lifestyle. Diabetes patients worldwide suffer from chronic wounds which seriously affect their daily life. Of particular interest here is that the incidence of chronic ulcers in people with diabetes mellitus is a common and significant problem in Thailand. The International Diabetes Federation (IDF) reported that 537 million people worldwide were reported to have diabetes in 2021.

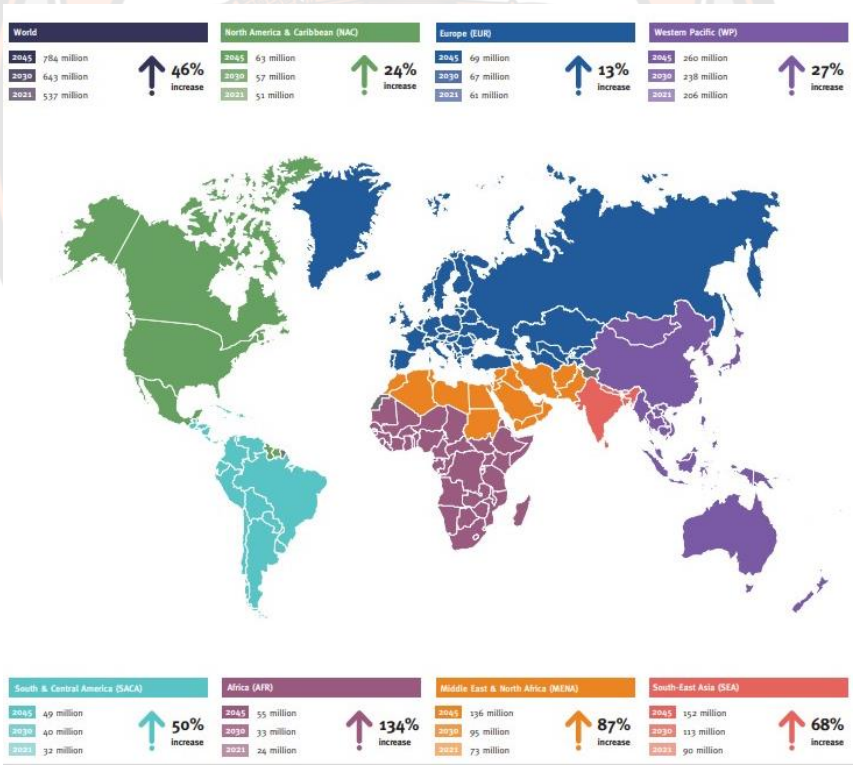

Figure 1 International Diabetes Federation (IDF), in 2021

Source: https://www.ncbi.nlm.nih.gov/pmc/articles/PMC7096556/

Any wounds have the possibility of becoming chronic. Therefore, wounds are categorized into four types based on their etiology, each having its usual location, depth, and appearance: venous, diabetic, and arterial ulcers. (Werdin et al., 2009) Chronic wounds are characterized as wounds that do not heal in the typical stages in an ordered and timely way and frequently fail in the inflammatory phase of healing. Despite variances in etiology at the molecular level, chronic wounds share some characteristics, including high levels of proinflammatory cytokines, proteases, ROS, and senescent cells, as well as persistent infection and a lack of stem cells, which are frequently dysfunctional (Frykberg & Banks, 2015).

However, in a state of high blood sugar, known as diabetes, the amount of collagen on the skin is less than average due to reduced collagen synthesis or stimulation of collagen degradation. (Black et al., 2003) Therefore, abnormalities in both quality (Schnider & Kohn, 1981) and quantity (Spanheimer et al., 1988) of collagen result in the wound healing process in diabetes being slow and incomplete (Goodson & TK, 1979). Inflammation is a process that occurs together with wound healing and is a complex response of the tissues to injury agents and damaged cells or damaged tissues. Evidence of inflammation is the presence of macrophage cells in the wound. (Hines et al., 1993; Roggin et al., 2001; Tracy Jr et al., 1996), as well as the presence of mediators in various types of inflammation. The mediators are secreted from plasma or certain cells as precursors to bind with specific receptors on cells involving inflammation, such as vanilloid-type transient receptor potential channels (TRPVs). All these mediators are induced to react differently to the inflammatory process depending on the type of mediator and the type of target cell; pain-causing mediators such as bradykinin and fever-causing mediators such as interleukin-1 (IL-1), IL-6, TNF-α (tumor necrosis factor- α), and prostaglandin. Many studies have shown that slow-healing diabetic ulcers are associated with chronic inflammation. (Pierce, 2001)

Wound management

Wound management has grown significantly as chronic wounds, and their associated disease prevalence has increased. Today, the biggest need in the treatment of chronic wounds is consensus-based information validated by practical experience

and supported by scientific data, which is easily conveyed and accessible to all wound care practitioners.

Initially, all chronic wounds should be treated using the TIME principle, which includes tissue debridement (safe for vascular ulcers), infection management, moisture balance, and edge effect. Following these general steps, the wound must be accurately diagnosed and categorized to provide appropriate care.

One method for reducing inflammation time is to use wound films which are appropriate for chronic wounds. Wound films are designed to keep pathogens out of the wound environment while promoting wound healing. The key requirements of wound films include absorption and removal of excessive drainage, allowing for oxygen exchange, prevention of trauma to newly formed tissue when removed, minimizing contamination, protection to fragile granulation tissue, pain reduction, no irritation, and the cost can be reasonable.

Herbs and natural products have traditionally been used for therapeutic reasons. The biological effects and safety of traditional plant products for human use have been demonstrated by observation over time, providing assurances of their safety to upcoming generations. Current scientific achievements prove and support traditional knowledge which provides significant benefits for human usage.

Silk fibroin

Silk farming is an important agricultural industry in Thailand. As well as being important for the textile industry, silk is currently being investigated for the development and production of medical materials such as scaffolds (Sofia et al., 2001; Unger et al., 2004) due to its mechanical properties in terms of being lightweight, significant strength, and elasticity. Silk is a protein product obtained from the cocoons of silkworms. The majority of the silk species in Thailand are *Bombyx mori*, a representative of Bombycidae. Typically, the main proteins in silk consist of fibroin and sericin Figure 2B. Fibroin is formed up of two major chains, a heavy (H-) chain (325 kDa) and a light (L-) chain (25 KDa), which are linked together by disulfide bonds to form the H-L complex Table 1. However, the problem with using silk as a medical material is the potential for allergic reactions to the sericin group protein (Soong & Kenyon, 1984; Wen et al., 1990; Zaoming et al., 1996). The extraction of silk to obtain only fibroin is therefore a necessary method to provide a material with

properties that can be as biocompatible, biodegradable, and non-inflammatory (Meinel et al., 2006; Meinel et al., 2005; Santin et al., 1999; Setzen & Williams 3rd, 1997; Wang et al., 2006) as other current medical materials.

Table 1 Structure of silk fiber

	Bombyx mori silkworm			
Silk fiber	Silk fibroin (72-81%)			Silk sericin (19-58%)
	H-chain	L-chain	P 25 glycoprotein	a glue-like protein
Molecular Weight	325 kDa	25 kDa	25 kDa	~300 kDa
Polarity	Hydrophobic			Hydrophilic
Structure	silk I (random-coil or unordered structure) silk II (crystalline structure) silk III (unstable structure)			non-crystalline structure
Function	the structural protein of fibers filament core protein			binds two fibroins together coating protein

Source: (Altman et al., 2003)

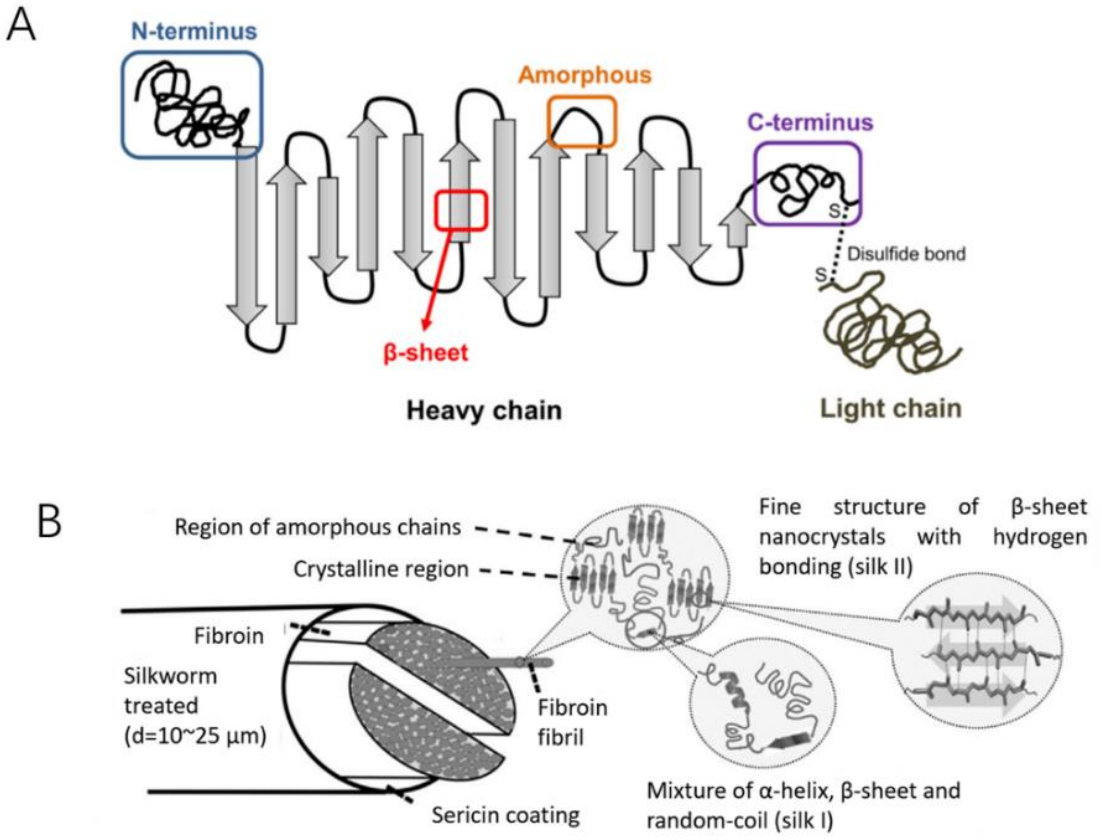

Figure 2 Schematic diagram of the silk structure. (A) heavy chain (i.e., N-terminus, β-sheets, Amorphous and C-terminus) and a light chain which is linked via disulphide bonds. (B) silkworm thread, fibril overall structure and silk fibroin polypeptide chains

The chemical structure of fibroin is composed of the hydrophobic block containing mostly small, branched structure amino acids such as glycine and alanine, and a hydrophilic block with long and charged branched structures of more complex amino acid sequences. Amino acids in the hydrophobic block have an orderly arrangement as crystals or beta-sheets due to the formation of hydrogen bonds between the amino acids resulting in silk protein having characteristic crystalline structure. The β-sheet regions are organized in parallel or anti-parallel arrangements, creating a stable and rigid structure. while amino acids in the hydrophilic block have a less orderly arrangement as amorphous Figure 2A. The combination of this orderly and unregulated structure makes fibroin both strong, flexible, and suitable to be used

as a medical material. It is also found that fibroin has water-absorbing properties that can allow cells to bind (adhesion property) which is an important step in the growth of adherent cells such as keratinocyte and fibroblast cells (Unger et al., 2004). It has also been found that during the growth of these cells on fibroin, they did not release cytokines such as IL-1β, TNF-α, or TGF- β1 (transforming growth factor- β1), which are inflammatory intermediates and a cause of fibrosis (Wang et al., 2006). On the other hand, they can stimulate the formation of bFGF and SMA, affecting wound healing (Inpanya et al., 2012).

Cannabidiol (CBD)

Hemp is a plant in the same family as cannabis (Cannabaceae) which is a traditional Thai herb that is receiving more attention because it has been found that different parts of hemp contain many critical active ingredients. The chemical structure of CBD was shown in Figure 3. The substance with the most outstanding properties is CBD with anti-inflammatory, analgesic (Hammell et al., 2016; Kaplan et al., 2008), antioxidant (Hampson et al., 1998), and anti-bacterial (Appendino et al., 2008; Van Klingeren & Ten Ham, 1976) activities. It has been used to treat diseases or symptoms related to inflammation, such as slow-healing diabetic ulcers associated with the occurrence of chronic inflammation. The mechanism of action of CBD is binding with cannabinoid receptors resulting in the inhibition of the secretion of various inflammatory mediators such as tumor necrosis factor and interleukins (Kaplan et al., 2008). It is an alternative medicine for the treatment of slow-healing wounds in leg ulcers with necrosis and small vascular obstruction. Furthermore, CBD can inhibit the secretion of inflammatory substances in the NF-kB pathway, and previous studies were conducted to inhibit the release of inflammatory media IL-8 and MMP-9.

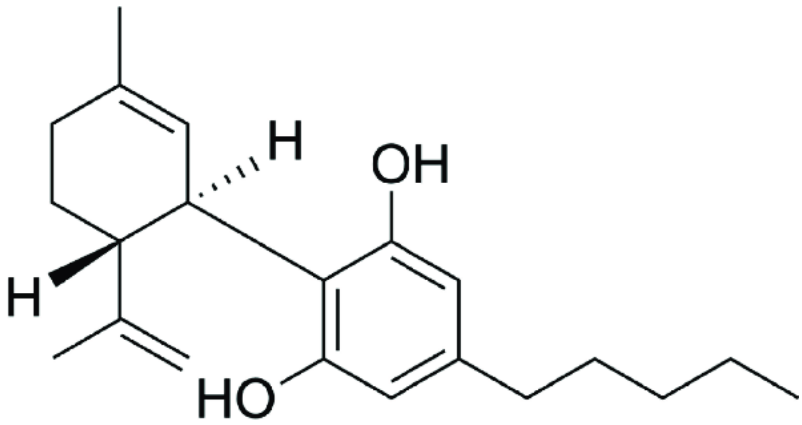

Figure 3 Chemical structure of cannabidiol (CBD)

Pharmacology and biochemistry of CBD

Although the actual mechanisms of the effects of CBD are not fully understood, CBD has been demonstrated to be an analgesic, anticonvulsant, muscle relaxant, anxiolytic, neuroprotective, antioxidant, and anti-inflammation properties. It has complicated pharmacological processes due to its wide range of activities, In addition to binding to endocannabinoid system CB1 and CB2 receptors. CBD stimulates the 5-HT1A serotonergic, TRPV1-2 vanilloid, and μ-opioid receptors. CBD also suppresses the activity of the fatty amide hydrolase (FAAH) and activates the inhibitory glycine receptor, both of which are involved in the inflammation-related healing process.

Mechanism of Action

CBD is binding with cannabinoid (CB) receptors of the endocannabinoid system, which are present all over the body, including the peripheral and central nervous systems and the brain. Many physiological reactions of the body are regulated by the endocannabinoid system, including pain, memory, appetite, and mood. CB1 receptors are present in the pain pathways of the brain and spinal cord, where they may impact CBD-induced analgesia and anxiolysis, whereas CB2 receptors are found on immune cells, where they may affect CBD-induced anti-inflammatory processes. CBD has been demonstrated to be a negative allosteric modulator of the cannabinoid CB1 receptor, the body's most abundant G-Protein

Coupled Receptor (GPCR). Allosteric regulation of a receptor occurs when a receptor's activity is changed on a functionally different area from the agonist or antagonist binding site. It is an alternative medicine for the treatment of slow-healing wounds in foot ulcers with necrosis and small vascular obstruction. Furthermore, cannabidiol extract will be able to inhibit the secretion of inflammatory substances in the NF-kB pathway, and previous studies have been conducted to investigate the inhibition of the release of inflammatory media IL-8 and MMP-9.

CHAPTER III

METHODOLOGY

Chemical and materials

1. Acrylamide (BIO-RAD Laboratories, Philadelphia, USA)
2. Ammonium sulfate ((NH4)2SO4, RCI Labscan, Bangkok, Thailand)
3. Amphotericin B (250 µg/ml) (Gibco, Invitrogen, Massachusetts, USA)
4. Bovine Serum Albumin BSA, Sigma-Aldrich Co, Missouri, USA)
5. Calcium chloride ($CaCl_2$, RCI Labscan, Bangkok, Thailand)
6. Cell proliferation kit II (2,3-bis (2-methoxy-4-nitro-5-sulphophenyl)-5-[(phenylamino)carbonyl]-2H-tetrazoliumhydroxide, XTT, Roche Diagnostics GmbH, Mannheim, Germany)
7. Coomassie brilliant blue (BIO-RAD Laboratories, Philadelphia, USA)
8. Dialysis membrane standard RC tubing (MWCO: 6-8 kDa) (Spectrum Laboratories, Inc., California, USA)
9. DC protein assay kit (BIO-RAD Laboratories, Philadelphia, USA)
10. Dimethyl Sulfoxide DMSO, Sigma-Aldrich Co, Missouri, USA)
11. Dulbecco's Modified Eagle's Medium (Sigma-Aldrich Co., Missouri, USA)
12. Ethanol 95% (Analytical grade, MERCK, Darmstadt, Germany)
13. Eosin (C.V. Laboratories Co., Ltd., Thailand)
14. Fluoromount G® (Southern Biotech, Alabama, USA)
15. Fetal bovine serum (Analytical grade, Gibco, California, USA)
16. Glycine (BIO-RAD Laboratories, Philadelphia, USA)
17. Hematoxylin (C.V. Laboratories Co., Ltd., Thailand
18. Hydrochloric acid (Labscan Asia Co., Ltd., Bangkok, Thailand)
19. Hydroxyproline Assay Kit (Sigma-Aldrich Co, Missouri, USA)
20. Lactic acid solution (88%) (Sigma-Aldrich Chemical GmbH, Germany
21. 2-Mercaptoethanol (BIO-RAD Laboratories, Philadelphia, USA
22. Sodium dodecyl sulfate (SDS) (BIO-RAD Laboratories, Philadelphia, USA
23. Sodium hydroxide (NaOH, RCI Labscan, Bangkok, Thailand

24. Triton X-100 (Sigma-Aldrich Co, Missouri, USA)
25. Tris-Hydrochloride (Promega Corporation, Madison, USA)
26. Tris-(Hydroxymethyl)-aminomethane (Analytical grade, MERCK, Darmstadt, Germany)
27. Trypan blue solution (Sigma-Aldrich Chemical GmbH, Steinheim, Germany)
28. 0.25% trypsin/0.01M EDTA (Sigma-Aldrich Co., Missouri, USA)
29. Penicillin/streptomycin solution (10,000 U/m) (Gibco, Invitrogen, Massachusetts, USA)
30. Muse Cell Cycle Assay Kit SDS (MERCK, Darmstadt, Germany)
31. 4,6-Diamidine-2-phenylindole dihydrochloride DAPI (Sigma-Aldrich Co, Missouri, USA)
32. Propidium Iodide PI, Sigma-Aldrich Co, Missouri, USA)
33. 4% Formaldehyde solution (Sigma-Aldrich Co, Missouri, USA)
34. Invitrogen™ Human VEGF ELISA Kit (Fisher Scientific, Denmark)

Instruments

1. Autoclave (HA-300P, Hirayama Manufacturing Corporation, Saitama, Japan)
2. Blender (HR2020, PHILIPS, Amsterdam, Netherlands)
3. Blood glucose monitoring system (Onetuch, horizon, Lifescan, Inc. California, USA)
4. Fourier transform infrared spectroscopy (FTIR spectrometer, Spectrum GX series, USA)
5. X-ray Diffractometry (XRD) BRUKER, D2 Phaser)
6. Field Emission Scanning electron microscopy (FE-SEM, ThermoFisher, Apreo S model, Hopkinton, MA, USA)
7. High Performance Liquid Chromatography (HPLC, Agilent 1260 Infinity II LC system)
8. Magnetic stirrer (Heidolph, MR3001, ITS group, Bangkok, Thailand)
9. Hot air oven (UFP800DW, MEMMERT, Schwabach, Germany)
10. Freeze dryer (FTS systems Dura dry type FD 95C12, LabX, Ontario, Canada)

11. Laminar flow (Class II-A/B3 Biological Safety Cabinet, BEC THAI, Bangkok, Thailand)

12. Incubator (VO400cool, MEMMERT, Schwabach, Germany)

13. pH meter (PL-700, Gondo, Nangang, Taiwan)

14. Conductivity Benchtop Meter (Lab 955, Xylem Analytics Germany Sales GmbH & Co. KG, WTW, Weilheim, Germany)

15. Microplate reader (Eon™, BioTek instrument, Vermont, USA)

16. Confocal microscope (A1 HD25/A1R HD25, Nikon®, Tokyo, Japan)

17. Flow cytometry (Guava®easyCyte, Merck Millipore, Massachusetts, USA)

Plant collection

Silkworm yellow cocoons

Silkworm yellow cocoons (*Bombyx mori* Linn., Nang-Laai strain) were kindly supplied by the Queen Sirikit Sericulture Center, Chiang Mai.

Cannabidiol (CBD)

Cannabidiol was isolated from *Cannabis Sativa* from the Bioscreening Unit of Naresuan University, and Cannabidiol crystalline solid was supplied by the Cayman Chemical Company (Ann Arbor, Michigan). (purity ≥ 95%, MW 314.5)

Preparation of silk fibroin extracts

The process for the preparation of silk fibroin was modified based on the previously reported protocols (Inpanya et al., 2012) and (Phimnuan et al., 2022). Briefly, the impurities were removed from the cocoon, which then cut into small pieces. The pieces of the silk cocoon were boiled at 85-90°C for 2h. The boiled silk cocoon was then degummed by boiling in 25 mM NaOH for 30 mins at 70°C. The degummed silk fibroin was rinsed three times with distilled water before drying in an oven at 50°C overnight and then boiled in 3M $CaCl_2$ at 85 - 90°C for 4-6 h at a ratio of 0.25 g degummed silk fibroin per 15 ml $CaCl_2$ solution. The fibroin solution was dialyzed in 15 mega ohm ultrapure water using molecular porous membrane tubing (MWCO: 6,000-8,000 Dalton) for 48h (change the water every 4-6 h). The dialyzed fibroin solution was then centrifuged at 8,000 rpm at 4°C for 15 mins to remove

insoluble debris. The clear fibroin solution was lyophilized by a freeze-drying procedure for 72h to produce the isolated fibroin, which was kept dry until use.

Characterization of isolated fibroin extract

Protein determination of the isolated fibroin

A DC protein assay kit was used to determine the protein concentration of the isolated fibroin extract. Bovine serum albumin (BSA), the reference protein, was diluted at various concentrations (0.125, 0.25, 0.50, 1.00, 2.00, 3.00, 4.00, and 5.00 mg/mL). The isolated fibroin extract was prepared at the concentration of 1 mg/ml, 5 µL of standard protein, and samples were pipetted into a 96-well plate. Then, 25 µL of reagent A (an alkaline copper tartrate solution) was added to each well, followed by 200 µL of reagent B (dilute Folin reagent) (BIO-RAD Laboratories, Philadelphia, USA). The standard protein and sample were incubated in the dark at room temperature (RT) for 15 mins and then measured at an absorbance of 750 nm by microplate spectrophotometer.

$$\text{Percentage of protein content} = \frac{\text{Concentration in the standard curve}}{\text{Concentration in the sample}} \times 100$$

Determination of the molecular weight pattern

The Sodium dodecyl sulfate-polyacrylamide gel electrophoresis (SDS-PAGE) method was used to check the molecular weight pattern. The isolated fibroin extract was analyzed by the SDS-PAGE method in 5% stacking gel and 12% separating gel. After electrophoresis, the gel was stained in Coomassie Brilliant Blue R-250 solution for 2h and de-stained with a de-staining solution (7% acetic acid, 10% methanol in water).

Fourier transform infrared spectroscopy (FTIR) analysis of the isolated fibroin

The FTIR spectroscopy technique was used to analyze the chemical composition of the isolated fibroin extract. The spectra were scanned over wavenumbers ranging from 4,000 cm^{-1} to 400 cm^{-1}.

Cannabidiol with 2-Hydroxypropyl-β-cyclodextrin (HP-β-CD) inclusion complexes (CBD complex)

Preparation of CBD with 2-hydroxypropyl-β-cyclodextrin complex

CBD and HP-β-CD were weighed in a 1:2 molar ratio, and the CBD and HP-β-CD were solubilized in 40% ethanol. The CBD solution was dropped constantly into

the HP-β-CD solution and then continuously stirred for 1 h before being filtered through 0.45μm membrane filters. Finally, the clear solution was lyophilized using freeze-drying for 48h and kept dry until use.

Quantification of cannabidiol in the CBD complex

The quantity of cannabidiol in the CBD complex was measured using high-performance liquid chromatography (HPLC) using an Agilent 1260 Infinity II LC System with G7129A 1260 vial sampler, G711A 1260 Quat pump VL, and G7115A 1260 DAD WR) together with the LC Open Lab software (offline), with 220 nm detection on a C18-packed column of 2.6 um, 4.6*150 mm. The mobile phase was composed of acetonitrile and 20 mM ammonium formate at pH 3.6. (75:25). After dissolving the CBD complex in the mobile phase, the solution was ultrasonically processed at room temperature for 40 min, and then filtered through a 0.45 μm membrane filter. The measurement of the CBD content in the solution was performed at a rate of 0.8 mL/min, at the injection amount of 5 μL, and run duration of 15 min. The quantity of cannabidiol was determined by integrating the peak with a calibration standard curve. All mobile phases were of HPLC quality.

FTIR analysis of CBD complex

The chemical properties of the CBD complex were observed by FTIR and recorded with an FTIR spectrophotometer between $4000\,cm^{-1}$ and $400\,cm^{-1}$ (Geskovski et al., 2021). The FTIR method is used to detect the changes in the characteristic peak location, frequency, and shape of the host-guest interaction of the groups of molecules and is commonly used to investigate the host-guest interaction in inclusion complexes (Pu et al., 2018). If CBD forms the complex with HP-β-CD, the characteristic peaks of CBD probably shift, decrease, or disappear.

Field emission scanning electron microscopy (FE-SEM) analysis

The FE-SEM provides topographical and elemental information at magnifications of 10X to 300,000X, with virtually unlimited depth of field. We used FE-SEM as an additional tool to confirm the development of inclusion complexes, to examine the morphology of the host and guest molecules, and the interaction of the CBD and HP-β-CD before and after inclusion. The CBD and HP-β-CD characteristic structures disappear totally in the inclusion complexes CBD/HP-β-CD which has a homogenous asymmetrical blocky

structure. These findings are compatible with the results of FTIR and HPLC, confirming that the inclusion complexes were formed successfully (Li et al., 2021).

X-ray diffraction (XRD)

The percentage of crystallinity and amorphous were measured by X-ray diffraction (XRD), Bruker, the D2 PHASER edition with the LYNXEYE XE-T detector system. The samples were mounted on a vitreous sample holder. The scan is kept a step size of 2θ = 10° to 80°.

Development of fibroin and CBD complex film (developed film)

Preparation of fibroin and CBD complex film

The preparation process for the fibroin extract and CBD complex film was optimized, and a simple casting technique was developed. The developed film was prepared by the blending of 600 mg of isolated fibroin extract and CBD complex containing 6.2 mg of CBD, which was dissolved in a lactic acid solution (pH 4.0±2) in a final volume of 15 mL. The solution was then stirred until homogeneous. The resultant solution was poured into a 6 x 6 cm silicone mold and dried at 47±2°C for 4h. The developed film was gently removed from the mold and stored in a dry and light-protected package until used.

Sterilization of the developed film

The developed films were sterilized by Ozone gas in an ozone box for 4h. Ozone gas has a high sterilizing capability against a wide range of bacteria (Gurley, 1985) and is attractive for this purpose due to its low cost and suitability for thermosensitive materials (Moat et al., 2009). The sterilized film was cut into the size of 1x1 cm^2 pieces which were immersed in 1 mL of DMEM serum-free, then incubated at 37˚C for 24 h. and then filtered through 0.45 µm membrane filters before being used in a later *in vitro* study.

Evaluation of the physicochemical properties developed film

The physical characteristics of the developed film, including surface and cross-section morphologies, were investigated. Tensile strength, elongation at break (%), and stability tests at the duration of time were evaluated.

FTIR analysis

The chemical structure of the developed film was identified using FTIR spectroscopy technique. The spectra were scanned across a range of wavenumbers from 4,000 cm^{-1} to 400 cm^{-1}.

Field emission scanning electron microscopy (FE-SEM) analysis

The surface and cross-sectional morphologies of the developed film was observed using a FE-SEM. The film was cut into 1x1 cm^2 and placed onto an aluminum stub using double-face adhesive tape before being sputter coated with ultrathin gold and examined with 5.0 KX magnification.

Mechanical properties

Tensile strength and percentage of elongation at break were determined using a tensometer contributed to the mechanical characteristics of the developed film and fibroin film. Tensile strength was used to evaluate matrix strength, and percentage of elongation at break was used to evaluate flexibility (Worasakwutiphong et al., 2021). The tensometer investigation conditions lists included a temperature of 25°C, humidity of 50%, load cell 20 N, separation speed of 0.5 mm/min, and size of 10 mm × 30 mm × 50 μm. The tensile strength and percentage of elongation at break were calculated using the following formula (Peh et al., 2000).

$$\text{Tensile strength (MPa)} = \frac{\text{Maximum force (N)}}{\text{Cross section area of sample (mm2)}} \times 100$$

$$\text{Elongation at break (\%)} = \frac{\text{Increase in length (mm)} \times 100}{\text{Initial length(mm)}}$$

The effect of the developed film on the biological functions of Normal Human Dermal Fibroblasts (NHDF) cell

Cell culture

Normal human dermal fibroblast (NHDF) cell lines (passages 8-15) were cultured in a culture flask in Dulbecco's Modified Eagle Medium (DMEM) mixed with 10% fetal bovine serum (FBS), 1% penicillin, and 1% streptomycin. The cells were incubated at 37°C in a humidified 5% CO_2 atmosphere and then kept in a culture medium for about one week, with the culture medium changed every 3 days. The cells

with an 80% proliferation rate were used in the experiment. The sterilized film of each sample was cut into the size of 1x1 cm^2 pieces which were immersed in 1 mL of DMEM serum-free before test.

Cytotoxicity test

A sodium 3'-[1-(phenylaminocarbonyl)-3,4-tetrazolium]-bis (4-methoxy6-nitro) benzene sulfonic acid hydrate) XTT assay was used to measure cell viability. The assay is based on the capacity of active mitochondria dehydrogenase to cleave the yellow tetrasodium salt XTT and produce an orange formazan product (Roslev & King, 1993). Briefly, NHDF cells ($1x10^4$ cells) were seeded in a 96-well plate and incubated in a humidified atmosphere of 5% CO_2 at 37°C for 24 h. The cells were washed with PBS before being further treated with the developed film solution 1 mL. After treating the NHDF cells, the incubated medium was discarded and replaced with the mixture of 200 µL of fresh serum-free medium and 50 µL of XTT reagent. The seeded cells were then incubated for 4h and the cell viability was then determined by measuring the absorbance at 490 nm with a microplate reader. The absorbance of the untreated cells (control group) was interpreted as representing 100% viability and an inverted microscope was used to observe the cell morphology. The experiment was performed in 3 replicates.

cell cycle analysis

The cell cycle is the series of procedures that occur within a cell that results in the duplication of DNA followed by cytokinesis in order to form two daughter cells. The cell cycle is tightly regulated and involves multiple checkpoints to ensure proper cell division and replication (Barnum & O'Connell, 2014). The Guava® Cell Cycle kit was used to determine the cell cycle phase (Merck Millipore, Canada). Briefly, the collected cells were fixed with 70% ethanol to form cell pellets which were incubated in 200 µL of propidium iodide (PI). In compliance with the manufacturer's recommendations, the cells were incubated in the dark at RT for 30 mins. Flow cytometry was used to determine the proportion of cells in each cell cycle phase, including G0/G1, S, and G2/M (Luangpraditkun et al., 2020)

Wound Healing Scratch Assay

The wound healing (or scratch) assay is a method used to measure two-dimensional cell migration. An artificial gap was generated on a confluent cell

monolayer using a culture-Insert 2 well, and movement was investigated via microscopy or other imaging. NHDF cells were seeded in culture-Insert 2 well at 2 × 10^5 cells/mL and incubated for 24 h. Then, treated with fibroin film and developed film solution 24 h. Wounds were created by moving the insert well out after the cells reached 100% confluence. After removing the media, cells were washed with 200 µL PBS, and 1 mL of samples were added to each well. Images were captured immediately following media replacement (T = 0) and every 12 h. for 48 h. using microscopy at 10X. The image was used to evaluate wound areas after the images were exported. In brief, a square tool was used to identify the wound area, and the extent of closure at T12, T24, T36, and T48.

Expression of growth factors by immunofluorescence

The Anti-VEGFA antibody was used to qualitatively evaluate the expression of vascular epidermal growth factor (VEGF) (ab39250, Abcam, Massachusetts, USA). In brief, NHDF cells (2x10^5 cells/well) were cultured in a cell culture slide at 37°C for 24 h. The cultured medium was then changed with a sample of the developed film solution and continually incubated for 24 h. At that time, the cells were fixed with 4% paraformaldehyde in PBS at RT for 10 mins followed by permeabilization with 0.1% Triton-X 100 for a further at room temperature 10 mins, then washed three times with PBS (5 minutes each time). The cells were then treated in a humidified environment at 4°C for 30 mins with 1% BSA and 22.52 mg/mL glycine in PBS-T to prevent non-specific antibody binding, followed by an overnight incubation with Anti-VEGFA antibody (diluted in 1% BSA in PBST). After washing with PBS 5 times (3 minutes each time), the cells were incubated at room temperature for 1 h in the dark with Alexa Fluor®488 conjugated secondary antibody (diluted in 1% BSA in PBST). The secondary antibody solution was replaced with PBS to wash the cells five times (3 minutes each time). After washing, the cells were incubated with 100 µL of DAPI (DNA stain) for 10 min before being washed again five times with PBS (3 minutes each time). After that, the cells were covered using an anti-fade mounting solution and examined with Laser scanning confocal microscopy (A1 HD25/A1R HD25, Nikon®, Tokyo, Japan).

The effect of the developed film on streptozotocin-induced diabetic rat models

Experiment animals

This study involved scientific experiments on animals. All animal research protocols utilized in this study were approved by Naresuan University Animal Care and Use Committee (NUACUC) - Application number NU- AE630714 before the study was conducted. Male Sprague-Dawley rats (6 weeks old and weight about 250 g) were used as an animal models. These animals were obtained from the Nomura Siam International Co., Ltd. Before the trial, all rats were acclimated to their new environment for 7 days, following IACUC guidelines.

Streptozotocin-induced diabetic rats

The animals were fasted for 16 h. before being diabetes-induced by a single intraperitoneal injection of 70 mg/kg streptozotocin (STZ) dissolved in 0.1M citrate buffer (pH 4). During the 3 days after the streptozotocin injection, the rats' blood glucose levels were monitored using a blood glucose monitor device. The animals having glucose levels exceeding 250 mg/dl were identified as diabetic-induced rats and used for further research (Akbarzadeh et al., 2007)

Wound creation

On day 7 after STZ induction, 1.5×1.5 cm of full-thickness skin wounds with a depth of 2.0 mm were carefully created on the back of each rat. This procedure was performed with the animals anesthetized with an intraperitoneal injection of thiopental 70-80 mg/kg body weight.

Treatment

After creating the wounds on the rats, they were randomly divided into 6 groups, with 5 rats in each group.

Group 1: non-diabetic rats without any treatment.

Group 2: non-diabetic rats with fibroin film.

Group 3: non-diabetic rats with fibroin/CBD film.

Group 4: diabetic rats without any treatment.

Group 5: diabetic rats with fibroin film.

Group 6: diabetic rats with fibroin/CBD film.

The sterilized film was applied to the wounds followed by a Tegaderm 3M as secondary film to cover the film to prevent bacterial infection.

Wound evaluation

The created wounds on the non-diabetic rats without treatment with the developed film (Group 1) and the diabetic rats without treatment with the developed film (Group 4) were used as the controls. After 7 days, all the rats were euthanized, and the wound sizes were observed and photographed.

Hematoxylin and Eosin Stain (H&E)

After surgical resection or biopsy, the tissues were embedded in a frozen section compound, fully submerging the tissue. The embedded tissue block can then be sectioned using a cryotome to obtain thin tissue sections for subsequent staining. Cut the tissue into thin sections (usually 4-5 µm thick) using a cryotome and mount them on microscope slides. Gradually rehydrate the tissue sections by rinsing them in decreasing concentrations of ethanol (100%, 95%, and 70%) for 1-2 minutes each. Immerse the slides in hematoxylin solution to stain the nuclei for 3-5 minutes. Rinse the slides with distilled water for 1-2 minutes to remove excess stain. Then, immerse the slides in eosin solution for 1-2 minutes to stain the cytoplasm and other tissue components. Rinse with distilled water for 1-2 minutes. Dehydrate the tissue sections by rinsing them with 95% ethanol for 1-2 minutes each. Clear the slides by immersing in xylene for 2-3 minutes to remove the ethanol and facilitate mounting. Finally, the slides were placed on a coverslip over the tissue sections using a mounting medium. Press down gently to remove any air bubbles and examine under the microscope. The nuclei should be stained blue with hematoxylin, and the cytoplasm and other tissue components should be stained pink to red with eosin, allowing for visualization of cellular details and tissue architecture.

Hydroxyproline assay

Hydroxyproline Assay Kit (colorimetric) ab222941 is designed to measure hydroxyproline content in tissue or protein/peptide hydrolysates. Briefly, the tissue samples were prepared by homogenizing 10 mg in 100 µL of water and transferred to a pressure-tight polypropylene vial with a PTFE-lined cap. The tissue samples were then hydrolyzed by adding 100 µL of concentrated hydrochloric acid (HCl, ~12M) at 120°C for 3 h. capped tightly, followed by neutralized with 100 µL of concentrated sodium hydroxide (NaOH, ~12M), and then centrifuged at 10,000 × g for 3 mins. Ten µL of the supernatant from the centrifuged samples were transferred

into a 96-well plate and dried at 60°C for 35 mins. Following the manufacturer's protocol, 100 µL of the Chloramine T/Oxidation Buffer Mixture was added to each sample and/or standard well and incubated at room temperature for 5 min. One hundred µL of the diluted DMAB reagent was then added to each sample and/or standard well and incubated at 60°C for 90 mins. Then, absorbance was measured at 560 nm using a spectrophotometer. The amount of hydroxyproline was expressed in µg/g tissue. The experiment was performed in triplicate per condition.

Statistical analysis

All data were expressed as the mean ± standard deviation. Hypothesis testing methods included analysis with the unpaired Student's t-test followed by the least significant difference (LSD) test; $p<0.05$ was considered to indicate statistical significance.

CHAPTER IV

RESULT AND DISCUSSION

Characteristics of the isolated fibroin extract

The isolated fibroin from silkworm cocoons (Nang-Laai strain) displayed yellowish cotton-like characteristics (Figure 4A). The isolated fibroin extract yielded approximately 68% w/w. The total protein content of the extract was 96.34 ± 0.14% w/w of the extract.

The molecular weight of the isolated fibroin was determined by the SDS-PAGE technique which is shown in Figure 4B. The isolated fibroin contains two bands of proteins, heavy chains with molecular weights ranging from 30 to 245 kDa and a light chain of 25 kDa. The broad smear bands result from the degradation of the heavy chain of raw silk protein. A specific band of the light chain is shown at approximately 25 kDa (Feng et al., 2020). A disulfide bond links the heavy chain and the light chain

The chemical functional groups of the isolated fibroin were determined using FTIR spectroscopy at the wavelength of 4000 - 400 cm^{-1}. Since silk fibroin is a protein composed of a sequence of amino acids, it contains amide I (C=O stretching), amide II (N-H bending) and amide III (in-phase combination of N-H in plane bending and C-N stretching) groups of amides on the backbone that can be observed by FT-IR and the results are shown in Figure 4C. The characteristic peaks of: Amide I from ester on the peptide backbone showed a frequency peak at 1696-1611 cm^{-1}, Amide II showed at 1550-1501 cm^{-1}, and Amide III showed at 1400-1200 cm^{-1}. In addition, the characteristic broad peak of N-H stretching and -OH stretching and strong hydrogen bond of protein chains of isolated fibroin was observed at 3600-3200 cm^{-1}.

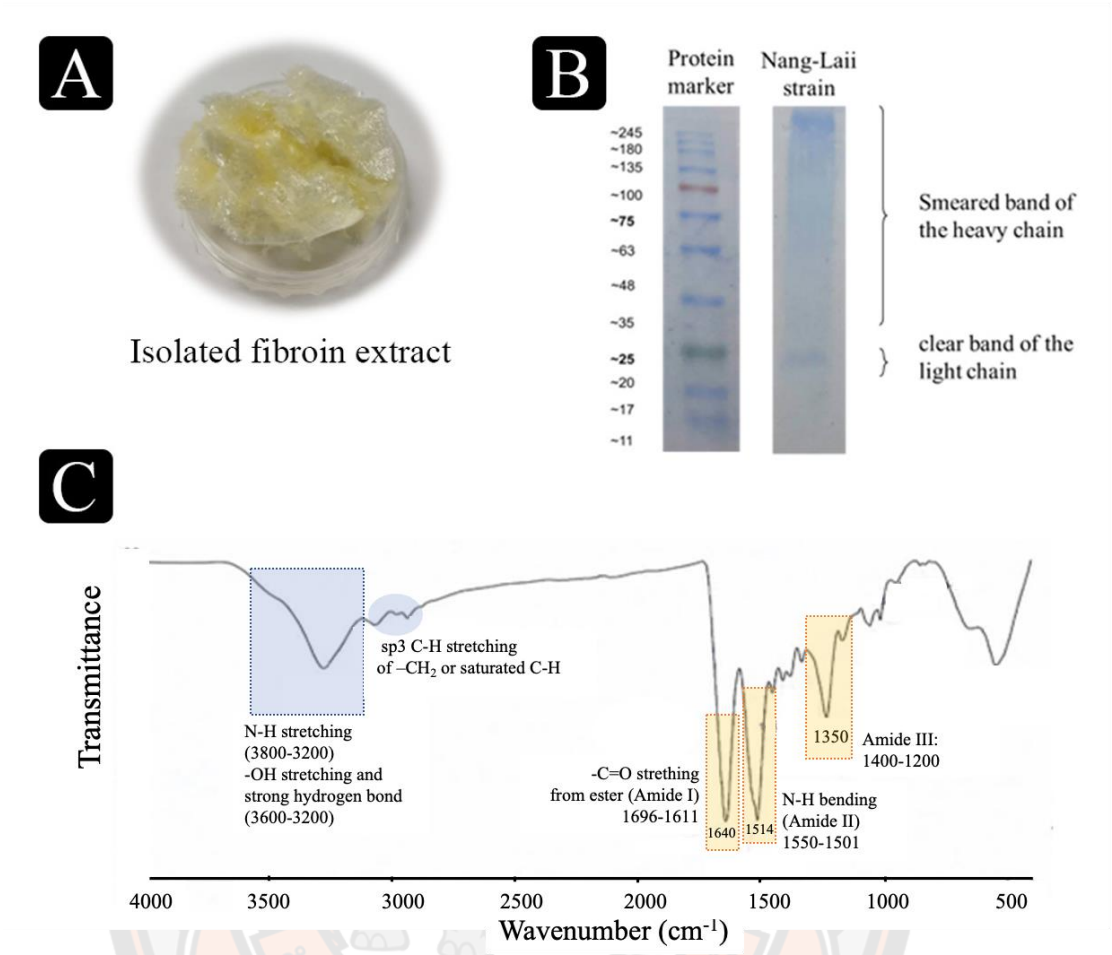

Figure 4 Physical characteristic (A) molecular weight patterns (B) and IR spectrum (C) of isolated fibroin extract

Physico-chemical characteristics and qualification of CBD complex

The inclusion complex technique was used to enhance the solubility and dispersibility of cannabidiol in the CBD complex. Figure 5A showed the appearance of a crystalline solid of the CBD complex as transparent and white crystal together with the chemical structure of CBD and 2-hydroxypropyl-β-cyclodextrin (HP-β-CD).

After the preparation of CBD with HP-β-CD to form CBD complex, the CBD complex was characterized by HPLC technique to determine the CBD content consisting in the CBD complex and the result shown in Figure 5B. The content of CBD was 81.5% w/w of CBD complex, according to the HPLC calibration curve generated from the standard CBD.

The chemical functional groups of the CBD complex were identified using FT-IR spectrometry in the frequency ranges of 4000 - 400 $cm^{-1}$and the results are shown in Figure 5C. This study was conducted to investigate the functional groups of the CBD complex comparing to that of CBD and HP-β-CD to confirm the successful preparation of CBD complex, in which the characteristic peaks of CBD or HP-β-CD are probably shifting, disappear or the formation of new functional groups were appeared. From results, the FT-IR characteristic peaks of CBD showed peaks mainly at 3550-3200 cm^{-1}, 3080 cm^{-1}, which are attributed to the -OH stretching and strong hydrogen bond and -C-H stretching of aromatic rings, respectively. Peaks at 2960, 2927, 2850 and 2825 cm^{-1} were corresponded to the -C-H stretching of methyl or methylene groups. The CBD characteristic peaks of -C=C stretching in aromatic ring were observed at 1646, 1605 and 1531 cm^{-1}. The other remarkable peaks at 1460 and 1240 cm^{-1} were observed, such as -OH bending and -C-O stretching, respectively. For HP-β-CD, a broad peak of -OH stretching and strong hydrogen bond was observed at 3650-3000 cm^{-1}. The -C-H stretching of methyl or methylene groups appeared at the same wavenumber as CBD but broader. The C-H bending of alkane, C-O stretching and strong peak of C-O-C stretching were observed at 1500-1238, 1175 and 1042 cm^{-1}, respectively. For CBD complex, the broad peaks of -OH stretching and strong hydrogen bond were observed at 3650-300 cm^{-1}, as expected mainly from HP-β-CD. A peak of C-H stretching was observed at the combinational frequency ranges of CBD and HP-β-CD. The peaks of C=O stretching (CBD), -OH bending (CBD), -C-H bending of alkane (HP-β-CD) and remarkable peak of C-O-C stretching (HP-β-CD) were observed at the same frequency ranges of either CBD or HP-β-CD. However, the peak of -C-H stretching of aromatic rings of CBD at 3080 disappeared from CBD complex. This suggested that the CBD, especially in part of aromatic rings (hydrophobic characteristic) had entirely entrapped by HP-β-CD and then restricted the vibration of the functional groups of CBD molecules. These findings demonstrated that CBD/HP-β-CD was successfully formed.

For surface morphology, Field Emission Scanning Electron Microscopy (FE-SEM) was utilized to examine the CBD complex. FE-SEM technique was used to confirm the development of inclusion complexes and to investigate their morphology before and after inclusion. The FE-SEM pictures of CBD, HP-β-CD, and CBD complex are shown in Figure 5D. The appearance of CBD was crystalline, with nubby

shapes of varying diameters. The prismatic crystal structure of HP-β-CD was observed in various sizes. The characteristics of CBD and HP-β-CD structures were changed completely as seen that CBD complex had a homogeneous, irregular blocky structure. The FE-SEM results were coincidence with the results of HPLC and FT-IR data which demonstrated that the inclusion complexes were formed effectively.

The crystalline structure of the complexation between CBD and HP-β-CD was investigated by XRD. When the inclusion complex was formed, the XRD pattern would not be the same peak of the HP-β-CD and crystalline structure of CBD because it would disrupt the crystalline nature of the CBD molecules. The individual XRD patterns of the HP-β-CD, CBD, and CBD inclusion complex were shown in Figure 5E. CBD showed crystalline characteristic peaks, especially at degrees of diffractions at 14.22, 15.37, 20.58, 22.13, 25.20 and 34.84. Whereas, the HP-β-CD showed a broad characteristic diffraction peak at 15.00-21.00 degree, representing its amorphous structure.

The diffraction peaks of CBD/HP-β-CD inclusion complexes differentiated from those of pure CBD and HP-β-CD. The inclusion complex did not represent simply a superposition of CBD and HP-β-CD, in which some crystalline peaks of CBD disappeared such as at 14.22, 22.13, 25.20, 34.84 degrees. The diffractive peaks in the CBD complex were observed to be shifted from crystalline characteristic peaks of neat CBD. In addition, the formation of two new diffractive peaks at 16.20 and 18.60 degrees were also observed. These results indicated that the CBD and HP-β-CD inclusion complex was successfully formed (Lv et al., 2019).

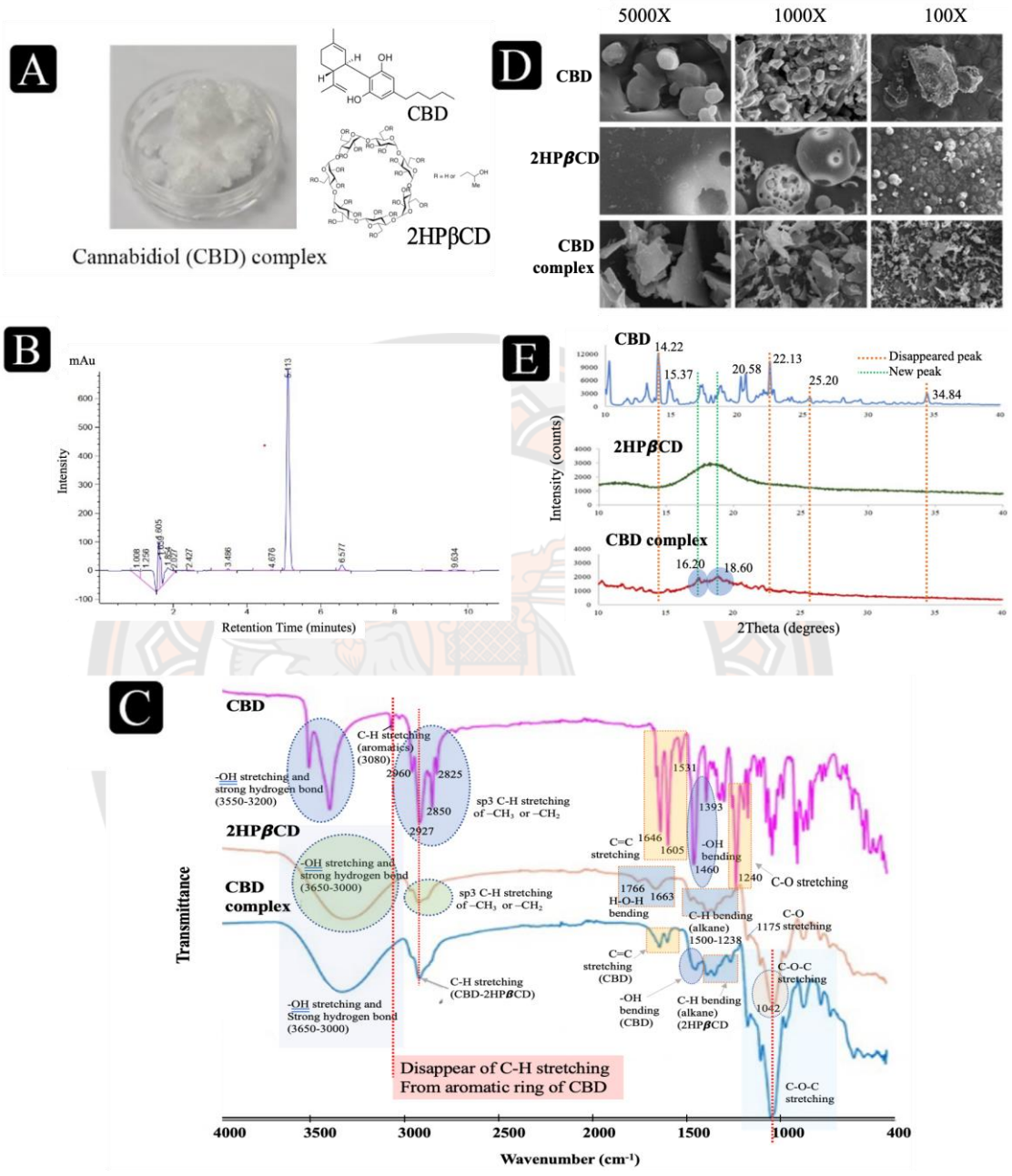

Figure 5 Physical appearance (A), HPLC of the chromatogram (B), FT-IR spectra (C), Field emission scanning electron microscopy (FE-SEM) (D), and X-ray diffractometer (XRD) (E) of CBD, HP-β-CD, and CBD complex

Characteristics of the blended fibroin/CBD complex film

Physico-chemical characteristics of blended fibroin/CBD complex film

The developed film was prepared by the casting film technique. Film appeared as transparent, yellowish, homogeneous, and flexible film, with the thickness of 50 μm, as shown in Figure 6A. The CBD content was 6.2 mg per film (36 cm^2). The developed film was characterized by its chemical functional groups using Fourier Transform Infrared Spectroscopy (FT-IR) technique. Field emission scanning electron microscopy (FE-SEM) was used to identify the morphology of the developed films. The mechanical properties (tensile strength and % elongation at break) of the developed films were also investigated.

Figure 6B demonstrated the FT-IR spectra of the isolated fibroin, the CBD complex, and the developed film in the frequency ranges from 4000 to 400 cm^{-1}. The FT-IR spectrum of the developed film was compared with that of isolated fibroin and CBD complex. As aforementioned, the characteristic peaks of isolated fibroin showed Amide I from ester on the peptide backbone at 1696-1611 cm^{-1}, Amide II at 1550-1501 cm^{-1}, and Amide III at 1400-1200 cm^{-1}. In addition, the characteristic broad peak of N-H stretching and -OH stretching and strong hydrogen bond of protein chains of isolated fibroin was observed at 3600-3200 cm^{-1}. For CBD complex, the broad peaks of -OH stretching and strong hydrogen bond were observed at 3650-3000 cm-1, as expected mainly from 2HP-β-CD. A peak of C-H stretching was observed at the combinational frequency ranges of CBD and 2HP-β-CD. The peaks of C=O stretching (CBD), -OH bending (CBD), -C-H bending of alkane (2HP-β-CD) and remarkable peak of C-O-C stretching (2HP-β-CD) were observed at the same frequency ranges of either CBD or 2HPβCD. The FT-IR spectrum of developed film simply showed spectrum of both isolated fibroin and CBD complex. The N-H stretching, -OH stretching and strong hydrogen bond peak was observed as the combination of the frequency broad peaks of isolated fibroin and CBD at 3650-3000 cm^{-1}. Interestingly, broader peaks of Amide I and Amide II and shifting peaks to higher wavenumbers of Amide II and C-O-C stretching were observed in developed film. The reason for the development of broader and shifted peaks is because of the formation of hydrogen bonding between isolated fibroin and CBD complex, which causes a change in the electron cloud that alters the resonant

frequency of that particular bond. This causes different molecules to have slightly different hydrogen bonding states leading to different frequencies and a broad band.

The crystallinity of blended film of fibroin and CBD complex inclusion was observed by powder X-ray diffraction analysis. Figure 6C illustrated the XRD pattern of CBD complex, isolated fibroin and developed film. As aforementioned, CBD complex were observed to be shifted from crystalline characteristic peaks of neat CBD and the formation of new peaks at 16.20 and 18.60 degrees were observed. Thus, the diffractive peaks of CBD complex were shown as sharp peaks at 15.37, 16.20, 18.60 and 20.58 degrees, indicating its crystal structure. Whereas isolated fibroin exhibited broad peaks and thus indicated as an amorphous structure. For developed film, the crystalline characteristic peaks of CBD complex were observed at approximately 21 degrees (shifting from neat CBD complex). In addition, other crystalline peaks of CBD complex (15.37, 16.20, 18.60 and 20.58 degree) disappeared. Two broader peaks were observed as they were characteristic XRD peaks of isolated fibroin. These results suggested that the molecular interaction and arrangement of molecules of CBD complex and isolated fibroin were altered when they were blended into the form of film.

For the mechanical properties, the tensile stress at maximum force of fibroin/CBD complex film was 48.67 ± 2.57 MPa and the % elongation at break at maximum force was 1.71 ± 0.21%, and the tensile stress at maximum force of fibroin film was 46.14 ± 2.81 MPa and the % elongation at break at maximum force was 1.51 ± 0.26% as shown in Figure 6D. The smooth surface of the fibroin/CBD film possibly functions as a guide through its particular interactions with the fibroin molecules. The fibroin typically produces beta-structure under shearing or elongating stress. Stronger adhesion between the two components should result from these interactions, providing composite materials with suitable tensile strengths.

After the preparation of isolated fibroin with CBD complex form to developed film. The CBD content was characterized by HPLC technique. The content of CBD was 100 $\mu g/cm^2$ of developed film, according to the HPLC calibration curve generated from the standard CBD as shown in Figure 6E.

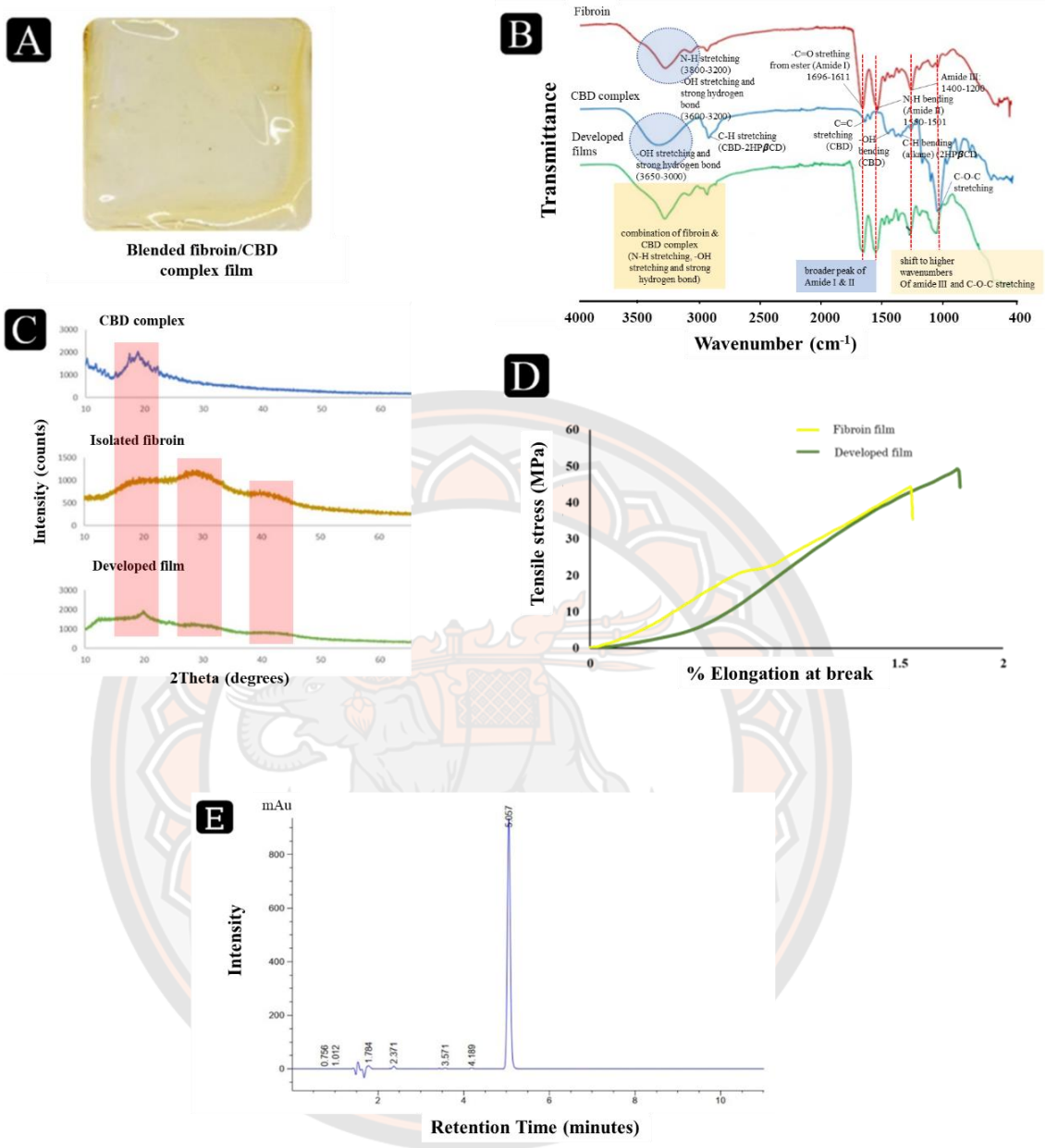

Figure 6 Physical appearance of developed film (A); FT-IR spectra of fibroin, CBD complex, and developed film (B); XRD patterns of fibroin, CBD complex, and developed film (C), tensile strength and % elongation at break of fibroin, and developed film (D), HPLC of the CBD content in developed film (E)

The morphology (surface and cross-section) of the fibroin/CBD film and fibroin film were observed using FE-SEM, as shown in Figure 7. Both films were relatively homogenous, indicating that the blend of fibroin with CBD complex was satisfactory conserved (Figure 7A and 7B). A noticeable difference was observed in the cross-section fractured by tensile pulling. The cross-sectional area of fibroin/CBD film was sharper compared to fibroin film indicating the brittle nature of the dry film and post-mixed fibroin with CBD complex would promote chain transformation (Figure 7C and 7D). Ductile, nanometer-scaled domains were observed, as seen in the form of elevated features with a size of 5 µm. The morphology of the internal structure in two types of film showed irregularity in ductile domains, indicating the fibrillar form of the internal assembly.

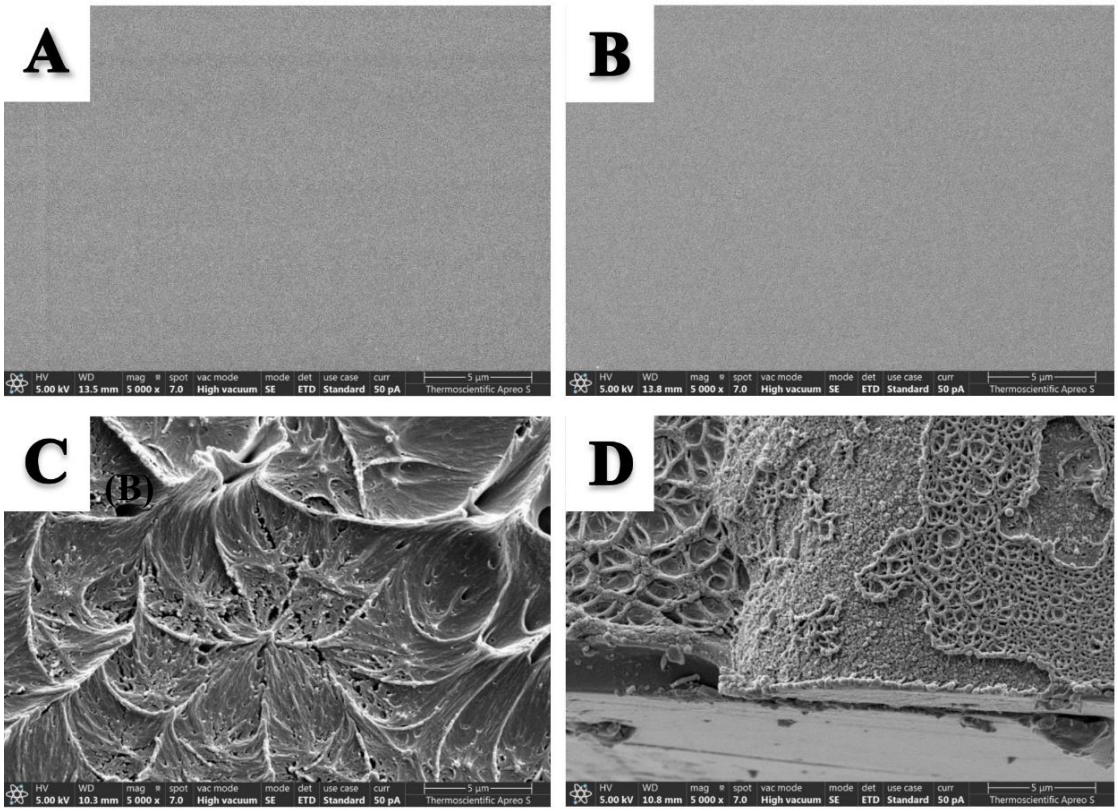

Figure 7 Field emission scanning electron microscopy (FE-SEM) images of developed film (A: surface; C: tensile fracture surface) and fibroin film (B: surface; D: tensile fracture surface)

Biological activities of blended fibroin/CBD complex film

in vitro study

Cytocompatibility

The report by (Hammell *et al.*, 2016) showed the effects of CBD in reducing inflammation in rats after receiving CBD transdermal gel at the concentration in various doses of 0.62, 3.1, 6.2, and 62.3 mg/day. The result showed that the effective doses were in the lower range of dosage (0.62, 3.1, 6.2 mg/day). Hence, the purpose of this research was to prepare the developed film which is designed to have CBD content in the dose of 6.2 mg/film which is the most effective dose based on the linear pharmacokinetic correlation. The developed film consisted of a fibroin content of 16.7 mg/cm^2 and the CBD was 0.17 mg/cm^2. The cytocompatibility of developed film was performed by XTT assay using NHDF. The results found that the developed film provided the percentage of viability of 146.46±5.34 which significantly higher than control group (untreaded NHDF) and fibroin film as 100±4.08 and 108.36±2.14 (p<0.001) as shown in Figure 8A. These results can be implied that the developed film had no negative effects on the viability and cell morphology of the treated cells Figure 8B.

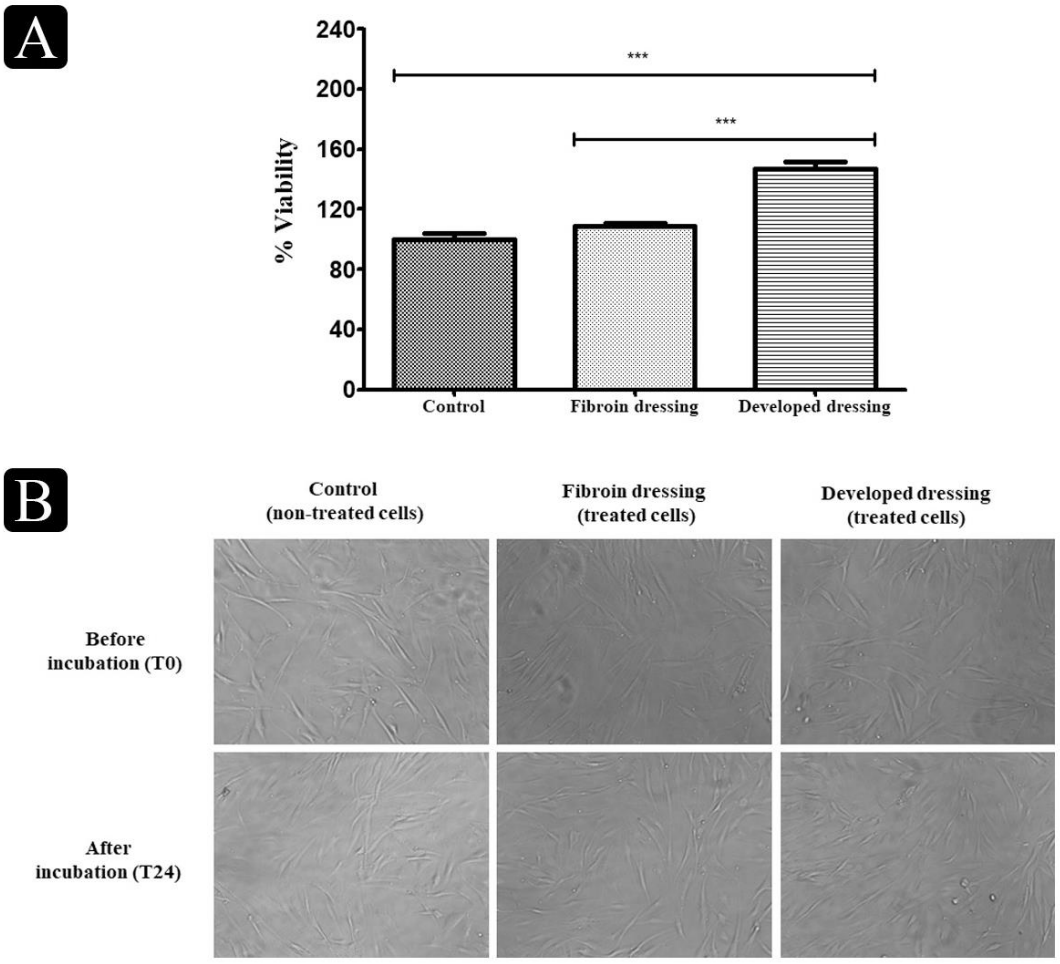

Figure 8 Percentage of cell viability of NHDF cells treated with fibroin film and developed film for 24 h (A). Data are expressed as percent of control group (untreated cells), and each column represents mean ± S.D in triplicate (n = 3); ***p<0.001. Cell morphology of NHDF treated with control group (untreated cell), fibroin film, and developed film at magnification of 20x (B)

Cell migration

In a scratch assay, a cell monolayer is grown to confluence in an insert 2-well which creates a wound and cell-free zone in the monolayer then cells can migrate. The recolonization of the scratched area is monitored to quantify cell migration. NHDF cells were cultured with DMEM with 0% FBS (control) and film

soaked in DMEM and then left for 48 h. The visualization of the scratching gap in film-treated cells (developed film) was almost completely healed at 48 h after scratch creation while the control group (untreated cells) was not healed simultaneously as shown in Figure 9. The therapeutic effects individually of fibroin and CBD can encourage the cell migration mentioned in the introduction.

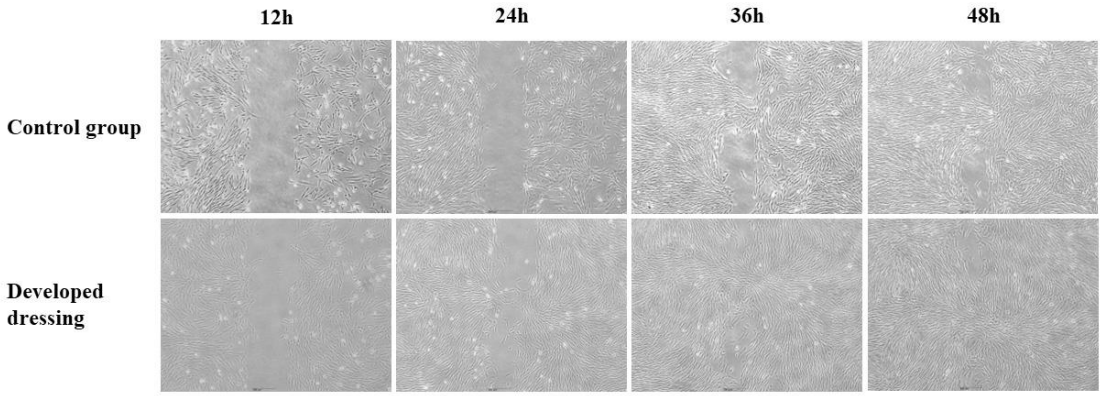

Figure 9 Cell migration of NHDF cells treated with the developed film at 12, 24, 36 and 48 h as compared to control group (untreated cells) at magnification of 10x

Cell cycle

This study evaluated the cell cycles of fibroin and developed films to those of a control group (non-treated cell). The cell cycle of the developed film was illustrated as flow cytometry dot plots and histogram profiles, as shown in Figure 10A. Briefly, the cells were cultured for 24 h followed by treated individually with fibroin and developed film for 24 h. The results found that cells treated with fibroin and developed film were initialed to stimulate cells in the phases of complete DNA synthesis and the phases of cell division (G2/M phases) increased by 20.06±1.00% and 25.02±2.13%, which was significantly higher than control group as 10.90±0.73% (p<0.001) as shown in Figure 10B. These results were distinctive correlated with our previous study as fibroin has also been found to have potential effects on the cell cycle process (Phimnuan et al., 2023). The cell cycle refers to the series of events that a cell goes through as it grows and divides into two daughter cells. The cell cycle is tightly

regulated and involves multiple checkpoints to ensure proper cell division and replication of genetic material. Also, CBD has been shown to possess anti-inflammatory properties, which can indirectly affect the cell cycle process. Inflammation can disrupt the normal cell cycle and promote abnormal cell growth. By reducing inflammation, CBD may help restore normal cell cycle regulation, promoting healthy cell division and preventing uncontrolled cell proliferation, indicating that the fibroin/CBD complex have potentials to promote cell cycle that involve on wound healing processes (Oláh et al., 2017).

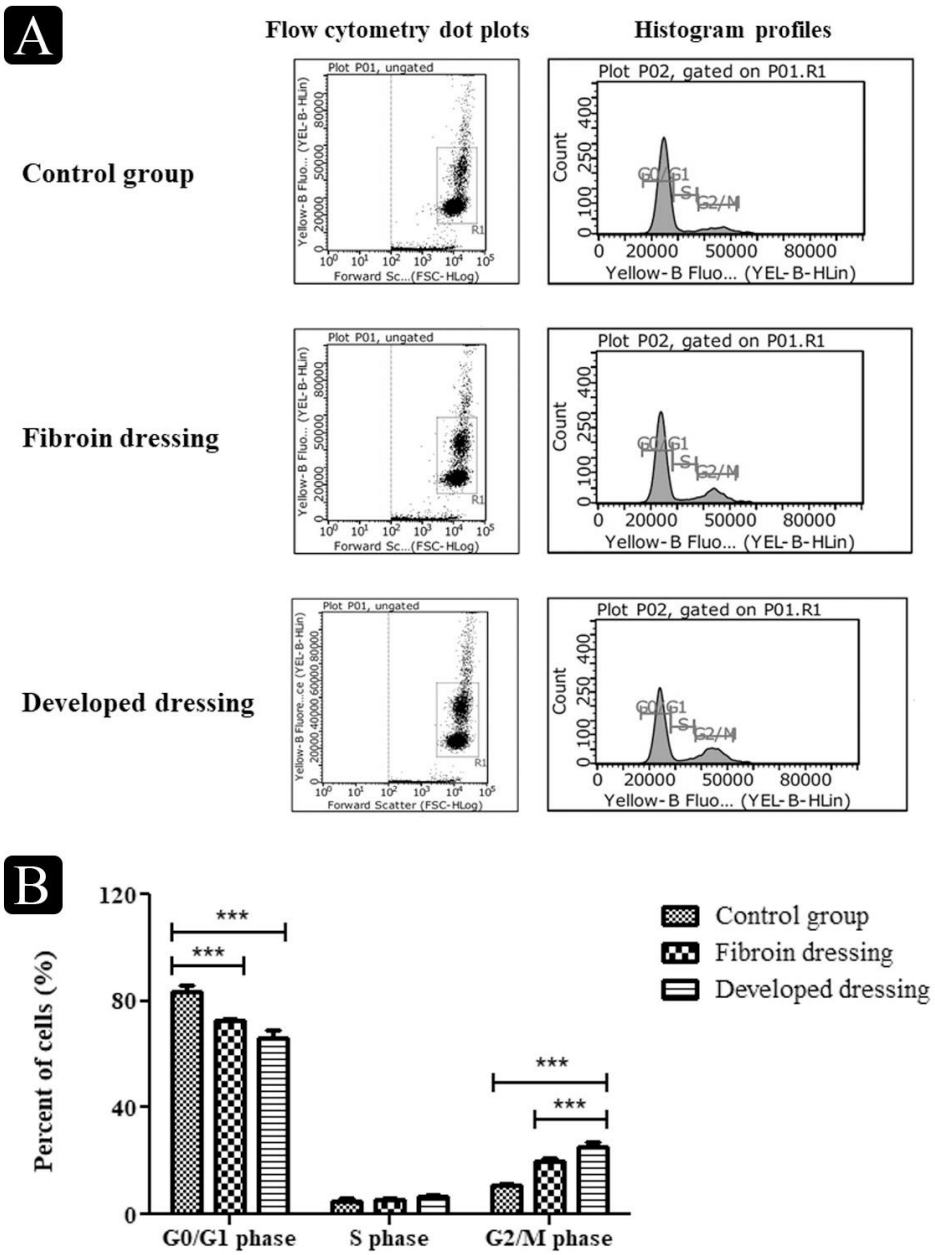

Figure 10 Cell cycle phases of NHDF cells treated with fibroin and developed film for 24 h compared to the control group (untreated cells). This figure shows the examples of cell cycle distribution in dot plots, histogram profiles (A) and percent of total cell (B), and each column represents mean ± S.D. in triplicate (n = 3); ***p<0.001

VEGF by immunoassay

The vasoactive properties of VEGF affected nuclear structural morphology and membrane fluidity were studied by confocal laser scanning microscopy (Figure 11). The blue dot of DAPI staining was used to determine the number of nuclei and one of blue refers to single cell due to the number of nuclei resulting in cell proliferation. The green color of Human VEGF Alexa Fluor® 488-conjugated antibody staining refers to membrane fluidity of cells. The results found that fibroin and developed film-treated cells promoted the nuclei due to therapeutic effects of fibroin results in cell proliferation. Fibroin has been shown to have potential for promoting cell proliferation. Fibroin can provide a supportive environment for cell growth and can stimulate cell proliferation through various mechanisms (Phimnuan et al., 2023). However, the developed film showed a higher membrane fluid area than control and fibroin group. It might be the potential of synergistic effect of fibroin and CBD. CBD can promote membrane fluidity in the context of the VEGF process by reducing oxidative stress, modulating lipid metabolism. Also, CBD has been found to interact with various membrane proteins which played a crucial role in maintaining the fluidity and function of cell membranes, including those involved in the VEGF pathway (Maccarrone et al., 2015).

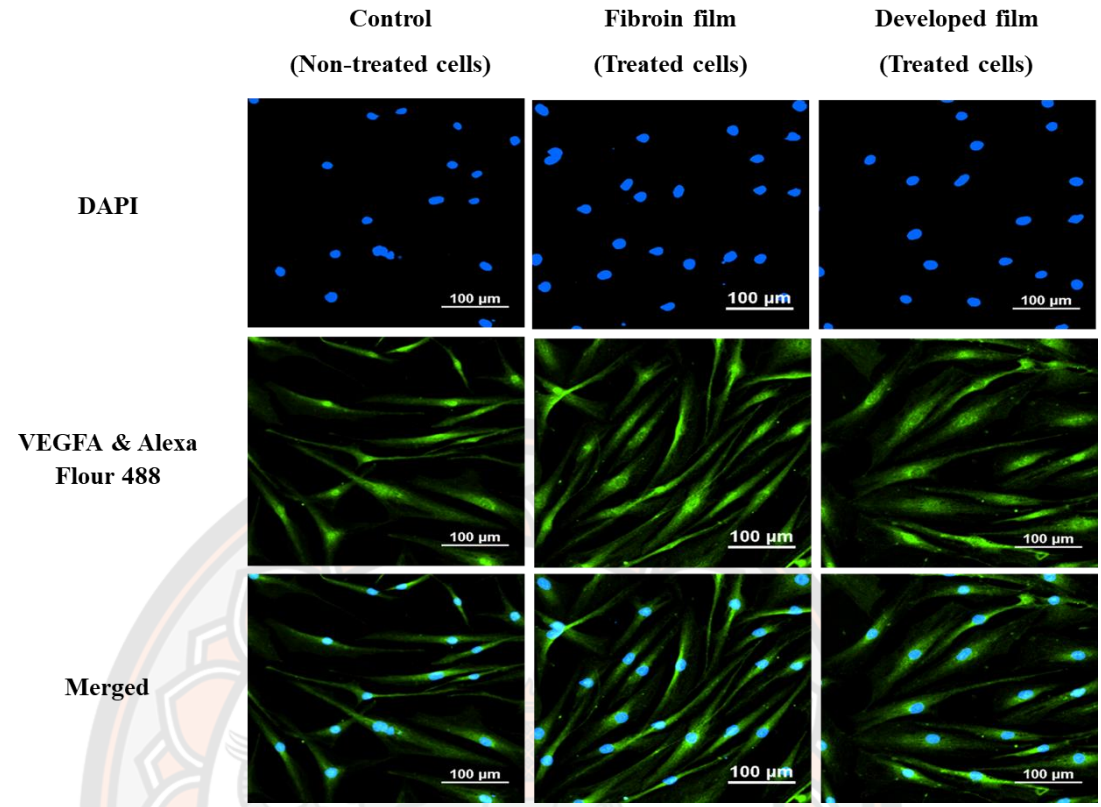

Figure 11 Immunofluorescence for VEGF expression of control group (untreated NHDF cells), fibroin and developed film at magnification of 20x

in vivo study

Wound evaluation

Wound size was evaluated in non-diabetic and diabetic rats at day 0 and day 7 after creating a standardized 1.5 x 1.5 cm full-thickness skin wound. At day 7, the percentage of wound contraction was not different in either group with or without treatment and in both non-diabetic and diabetic rats. In addition, those wounds treated with developed film appear to be drier and smaller than the non-treated wounds as shown in Figure 12.

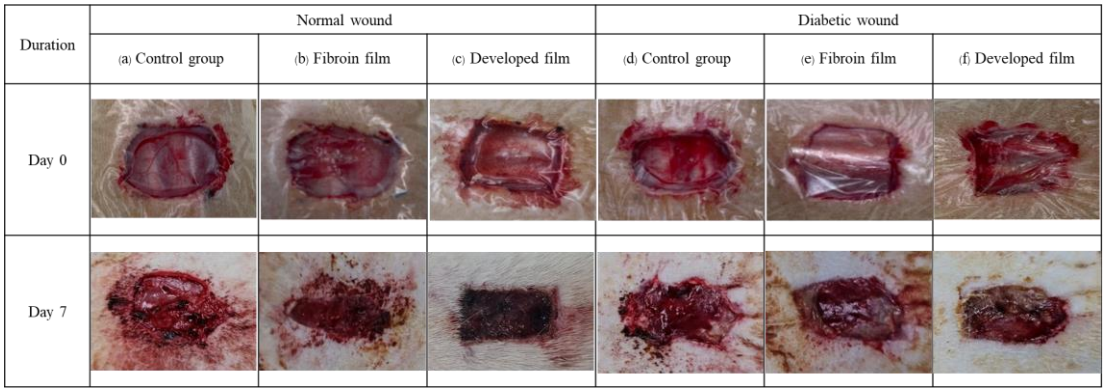

Figure 12 Photographs of wound contraction in the control group (non-treated wound), fibroin film and developed film in both of non-diabetic and diabetic rats at days 0 and 7

Hematoxylin and Eosin (H&E) staining

To determine the changes produced in the wound after being treated with fibroin film and developed film during the skin regeneration processes as shown in Figure 10. The histological findings of skin wound sections, regarding re-epithelialization and final configuration of the dermal layer, were comparable with the control group (non-created wound) and fibroin film or developed film (treated wound) as shown in Figure 13. Although, in the treated wound groups the re-epithelialization was not completed after 7 days, the appearance of wound appeared to be different in the characterized by epidermis and a dermis composed by a dense and regular connective tissue. In the control group Figure 13 (A, D), the re-epithelialization well-formed a dense of regular of connective tissue. In the other hand, the re-epithelialization displayed the dermis was mainly composed of poorly dense connective tissue with a regular configuration in both treated groups with fibroin and developed film. One of the changes that can occur in the epidermis and dermis of a diabetic wound is an increase in the deposition of collagen, a type of connective tissue. The results described as the formation of dense and regular connective tissue in the wound bed, which may contribute to delayed healing and increased scarring. The increase of collagen deposition in diabetic wounds may be due to a variety of factors, including alterations in the local cytokine and growth factor environment, decreased

oxygen supply to the wound bed, and changes in the activity of cells that produce collagen, such as fibroblasts. Overall, the dense and regular connective tissue observed in the epidermis and dermis of diabetic wounds is likely a result of the complex interplay between these and other factors and may contribute to the impaired healing observed in these wounds (Patel et al., 2019).

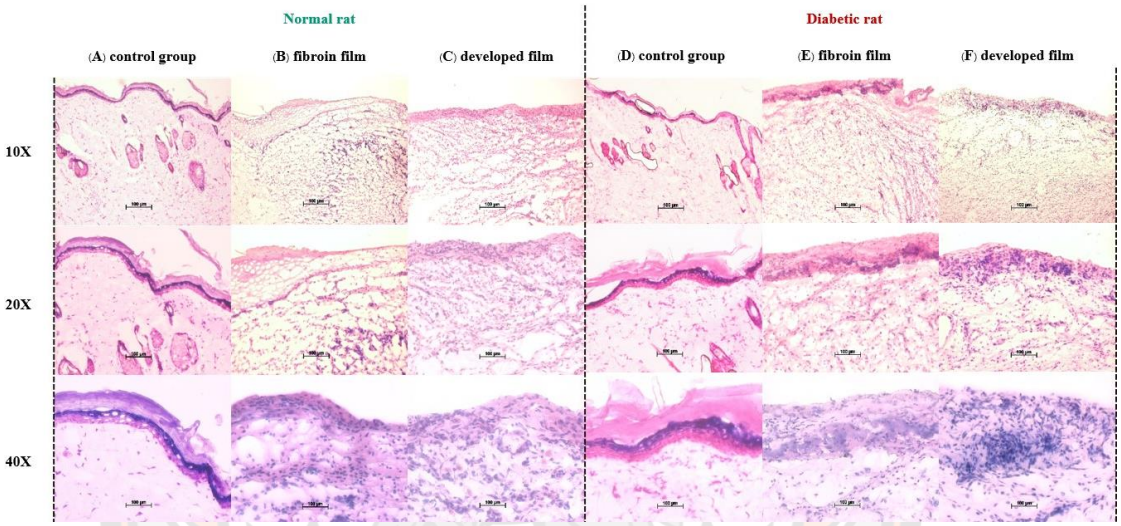

Figure 13 Histological assessment of wound healing by hematoxylin and eosin (H&E) staining. control groups (non-created wound) (A, D); fibroin film (B, E); developed film (C, F). Scale bar 100 µm

Hydroxyproline assay

The determination of hydroxyproline secretion of the control group (non-treated wound), fibroin film and developed film in non-diabetic-induced and diabetic-induced rats for 7 days (Figure 14). Hydroxyproline assay: that both the non-diabetic and diabetic rats treated with fibroin/CBD film provided a hydroxyproline content of 27.7±1.5 and 44.0±2.0 µg/g of tissue and treated with fibroin film provided a hydroxyproline content of 68.3±6.0 and 76.0±14.5 µg/g of tissue which was significantly higher than the non-treated group as 20.7±3.2 and 33.3±1.2 µg/g of tissue. In diabetic rats had several factors that can lead to higher hydroxyproline levels in wounds compared to non-diabetic rats. Diabetic rats can cause increased oxidative stress, which can stimulate collagen synthesis and lead to enhanced hydroxyproline

levels (Martins et al., 2021). Additionally, diabetic rats can have impaired degradation of collagen, which can also contribute to higher hydroxyproline levels (Bermudez et al., 2011).

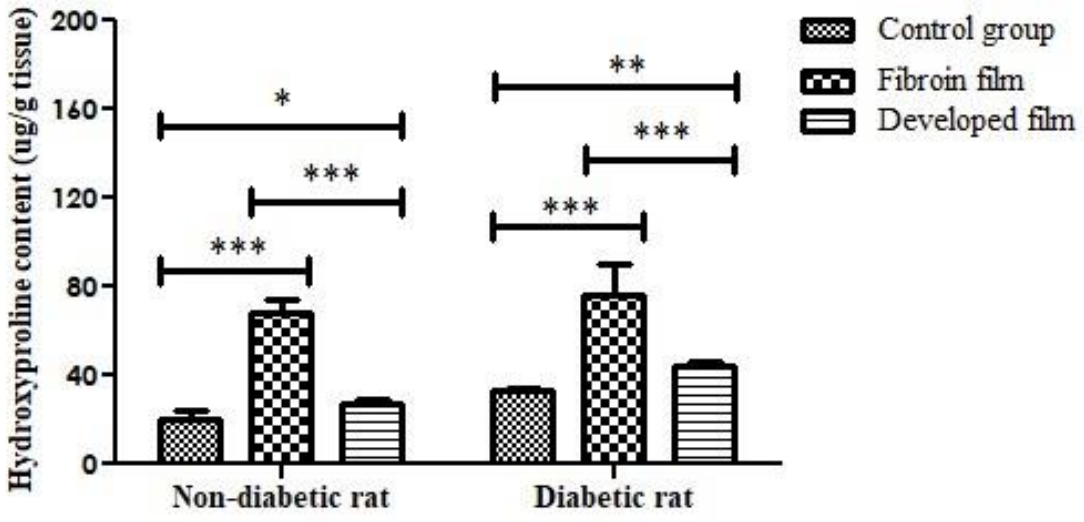

Figure 14 The determination of hydroxyproline secretion of the control group (non-treated wound), fibroin film and developed film in non-diabetic-induced and diabetic-induced rats for 7 days. Data are expressed as hydroxyproline content (µg/g tissue), and each column represents mean ± S.D. in triplicate (n=3); *** p<0.001

CHAPTER V

CONCLUSIONS

In this study, the development of the blended fibroin/hemp CBD film for the treatment of chronic wounds could be suitable for further clinical experiments according to the potential activity of this film in In vitro and In vivo test.

In this study, the isolated fibroin from silkworm cocoons (Nang-Laai strain) displayed yellowish cotton-like characteristics. The total protein content of the extract was 96.34 ± 0.14% w/w. The purity of the isolated fibroin was confirmed using the molecular weight by SDS-PAGE at specific band of the light chain shown at approximately 25 kDa and the chemical structure of amide I, II, and III by FT-IR.

The characteristics of inclusion complexes of cannabidiol (CBD) with 2-Hydroxypropyl-β-cyclodextrin (HP-β-CD) to form CBD complex displayed in the crystal white power. The quantity of cannabidiol content in the CBD complex was measured using high-performance liquid chromatography (HPLC) showed a CBD content of 273 micrograms/1 mg of CBD complex and their structural analysis using FTIR spectrophotometry, X-ray diffraction, and topography by FE-SEM. All the results of inclusion complexes indicate that the HP-β-CD can encapsulate the CBD molecules. The study suggests the CBD inclusion complex has the potential for solubility indicating that CBD compound can mix well with other soluble substances.

The developed film that was prepared using the casting film technique appeared transparent, golden in color, homogeneous, and flexible. The CBD content was 6.2 mg/sheet. Investigate in in vitro and in vivo study, the blended fibroin/hemp CBD film can be a promising therapeutic approach in the treatment of chronic wounds. The film enhances cell proliferation and migration, vascular epidermal growth factor (VEGF) secretion, and no toxicity in the NHDF cell. The practical implications of this animal study are that the blended fibroin/CBD hemp film can be a potential therapeutic approach for treating chronic wounds. The film can enhance the healing rate of the diabetic wound in rats model by promoting hydroxyproline leading to increase collagen synthesis and promoting the wound drier and more compact. The

use of natural products in wound healing can be a safer and more effective alternative to traditional treatments.

REFERENCES

Akbarzadeh, A., Norouzian, D., Mehrabi, M. R., Jamshidi, S., Farhangi, A., Verdi, A. A., Mofidian, S. M., & Rad, B. L. (2007). Induction of diabetes by Streptozotocin in rats. *Indian Journal of Clinical Biochemistry*, *22*(2), 60-64. https://doi.org/10.1007/bf02913315

Appendino, G., Gibbons, S., Giana, A., Pagani, A., Grassi, G., Stavri, M., Smith, E., & Rahman, M. M. (2008). Antibacterial cannabinoids from Cannabis sativa: a structure− activity study. *Journal of natural products*, *71*(8), 1427-1430.

Barnum, K. J., & O'Connell, M. J. (2014). Cell cycle regulation by checkpoints. *Methods in Molecular Biology*, *1170*, 29-40. https://doi.org/10.1007/978-1-4939-0888-2_2

Bauer, S. M., Bauer, R. J., & Velazquez, O. C. (2005). Angiogenesis, vasculogenesis, and induction of healing in chronic wounds. *Vascular and Endovascular Surgery*, *39*(4), 293-306. https://doi.org/10.1177/153857440503900401

Bermudez, D. M., Herdrich, B. J., Xu, J., Lind, R., Beason, D. P., Mitchell, M. E., Soslowsky, L. J., & Liechty, K. W. (2011). Impaired Biomechanical Properties of Diabetic Skin: Implications in Pathogenesis of Diabetic Wound Complications. *The American journal of pathology*, *178*(5), 2215-2223. https://doi.org/https://doi.org/10.1016/j.ajpath.2011.01.015

Black, E., Vibe-Petersen, J., Jorgensen, L. N., Madsen, S. M., Ågren, M. S., Holstein, P. E., Perrild, H., & Gottrup, F. (2003). Decrease of collagen deposition in wound repair in type 1 diabetes independent of glycemic control. *Archives of surgery*, *138*(1), 34-40.

Cheng, K.-Y., Lin, Z.-H., Cheng, Y.-P., Chiu, H.-Y., Yeh, N.-L., Wu, T.-K., & Wu, J.-S. (2018). Wound healing in streptozotocin-induced diabetic rats using atmospheric-pressure argon plasma jet. *Scientific reports*, *8*(1), 1-15.

DiPietro, L. A., & Polverini, P. J. (1993). Role of the macrophage in the positive and negative regulation of wound neovascularization. *Behring-Institute-Mitteilungen* (92), 238-247.

Eming, S. A., Krieg, T., & Davidson, J. M. (2007). Inflammation in wound repair: molecular and cellular mechanisms. *Journal of Investigative Dermatology*, *127*(3), 514-525. https://doi.org/10.1038/sj.jid.5700701

Feng, Y., Lin, J., Niu, L., Wang, Y., Cheng, Z., Sun, X., & Li, M. (2020). High Molecular Weight Silk Fibroin Prepared by Papain Degumming. *Polymers*, *12*(9), 2105. https://www.mdpi.com/2073-4360/12/9/2105

Frykberg, R. G., & Banks, J. (2015). Challenges in the Treatment of Chronic Wounds. *Advances in wound care (New Rochelle)*, *4*(9), 560-582. https://doi.org/10.1089/wound.2015.0635

Geskovski, N., Stefkov, G., Gigopulu, O., Stefov, S., Huck, C. W., & Makreski, P. (2021). Mid-infrared spectroscopy as process analytical technology tool for estimation of THC and CBD content in Cannabis flowers and extracts. *Spectrochimica Acta Part A: Molecular and Biomolecular Spectroscopy*, *251*, 119422. https://doi.org/https://doi.org/10.1016/j.saa.2020.119422

Goodson, W., & TK, H. (1979). Wound healing and the diabetic patient.

Greenhalgh, D. G. (1998). The role of apoptosis in wound healing. *The International Journal of Biochemistry & Cell Biology*, *30*(9), 1019-1030. https://doi.org/10.1016/s1357-2725(98)00058-2

Gurley, B. (1985). Ozone: pharmaceutical sterilant of the future? *PDA Journal of Pharmaceutical Science and Technology*, *39*(6), 256-261.

Gurtner, G. C., & Evans, G. R. (2000). Advances in head and neck reconstruction. *Plastic and Reconstructive Surgery*, *106*(3), 672-682; quiz 683.

Gurtner, G. C., Werner, S., Barrandon, Y., & Longaker, M. T. (2008). Wound repair and regeneration. *Nature*, *453*(7193), 314-321. https://doi.org/10.1038/nature07039

Hammell, D., Zhang, L., Ma, F., Abshire, S., McIlwrath, S., Stinchcomb, A., & Westlund, K. (2016). Transdermal cannabidiol reduces inflammation and pain-related behaviours in a rat model of arthritis. *European Journal of Pain*, *20*(6), 936-948.

Hampson, A., Grimaldi, M., Axelrod, J., & Wink, D. (1998). Cannabidiol and (−) Δ9-tetrahydrocannabinol are neuroprotective antioxidants. *Proceedings of the National Academy of Sciences*, *95*(14), 8268-8273.

Hines, J. E., Johnson, S. J., & Burt, A. (1993). In vivo responses of macrophages and perisinusoidal cells to cholestatic liver injury. *The American journal of pathology*, *142*(2), 511.

Inpanya, P., Faikrua, A., Ounaroon, A., Sittichokechaiwut, A., & Viyoch, J. (2012). Effects of the blended fibroin/aloe gel film on wound healing in streptozotocin-induced diabetic rats. *Biomedical Materials*, *7*(3), 035008.

Kaplan, B. L., Springs, A. E., & Kaminski, N. E. (2008). The profile of immune modulation by cannabidiol (CBD) involves deregulation of nuclear factor of activated T cells (NFAT). *Biochemical pharmacology*, *76*(6), 726-737.

Koh, T. J., & DiPietro, L. A. (2011). Inflammation and wound healing: the role of the macrophage. *Expert Reviews in Molecular Medicine*, *13*, e23. https://doi.org/10.1017/s1462399411001943

Li, H., Chang, S.-L., Chang, T.-R., You, Y., Wang, X.-D., Wang, L.-W., Yuan, X.-F., Tan, M.-H., Wang, P.-D., & Xu, P.-W. (2021). Inclusion complexes of cannabidiol with β-cyclodextrin and its derivative: Physicochemical properties, water solubility, and antioxidant activity. *Journal of Molecular Liquids*, *334*, 116070.

Luangpraditkun, K., Charoensit, P., Grandmottet, F., Viennet, C., & Viyoch, J. (2020). Photoprotective Potential of the Natural Artocarpin against In Vitro UVB-Induced Apoptosis. *Oxidative Medicine and Cellular Longevity*, *2020*, 1042451. https://doi.org/10.1155/2020/1042451

Lv, P., Zhang, D., Guo, M., Liu, J., Chen, X., Guo, R., Xu, Y., Zhang, Q., Liu, Y., Guo, H., & Yang, M. (2019). Structural analysis and cytotoxicity of host-guest inclusion complexes of cannabidiol with three native cyclodextrins. *Journal of Drug Delivery Science and Technology*, *51*, 337-344. https://doi.org/https://doi.org/10.1016/j.jddst.2019.03.015

Maccarrone, M., Bab, I., Bíró, T., Cabral, G. A., Dey, S. K., Di Marzo, V., Konje, J. C., Kunos, G., Mechoulam, R., Pacher, P., Sharkey, K. A., & Zimmer, A. (2015). Endocannabinoid signaling at the periphery: 50 years after THC. *Trends in Pharmacological Sciences*, *36*(5), 277-296. https://doi.org/10.1016/j.tips.2015.02.008

Madden, J. W., & Peacock, E. E., Jr. (1971). Studies on the biology of collagen during wound healing. 3. Dynamic metabolism of scar collagen and

remodeling of dermal wounds. *Annals of Surgery*, *174*(3), 511-520. https://doi.org/10.1097/00000658-197109000-00017

Martin, P. (1997). Wound healing--aiming for perfect skin regeneration. *Science*, *276*(5309), 75-81.

Martins, S. G., Zilhão, R., Thorsteinsdóttir, S., & Carlos, A. R. (2021). Linking Oxidative Stress and DNA Damage to Changes in the Expression of Extracellular Matrix Components. *Frontiers in Genetics*, *12*, 673002. https://doi.org/10.3389/fgene.2021.673002

Oláh, A., Szekanecz, Z., & Bíró, T. (2017). Targeting Cannabinoid Signaling in the Immune System: "High"-ly Exciting Questions, Possibilities, and Challenges. *Frontiers in Immunology*, *8*, 1487. https://doi.org/10.3389/fimmu.2017.01487

Patel, S., Srivastava, S., Singh, M. R., & Singh, D. (2019). Mechanistic insight into diabetic wounds: Pathogenesis, molecular targets and treatment strategies to pace wound healing. *Biomedicine & Pharmacotherapy*, *112*, 108615. https://doi.org/https://doi.org/10.1016/j.biopha.2019.108615

Peh, K., Khan, T., & Ch'ng, H. (2000). Mechanical, bioadhesive strength and biological evaluations of chitosan films for wound dressing. *Journal of Pharmacy & Pharmaceutical Sciences*, *3*(3), 303-311.

Phimnuan, P., Dirand, Z., Tissot, M., Worasakwutiphong, S., Sittichokechaiwut, A., Grandmottet, F., Viyoch, J., & Viennet, C. (2023). Beneficial Effects of a Blended Fibroin/Aloe Gel Extract Film on the Biomolecular Mechanism(s) via the MAPK/ERK Pathway Relating to Diabetic Wound Healing. *ACS Omega*, *8*. https://doi.org/10.1021/acsomega.2c07507

Phimnuan, P., Worasakwutiphong, S., Sittichokechaiwut, A., Grandmottet, F., Nakyai, W., Luangpraditkun, K., Viennet, C., & Viyoch, J. (2022). Physicochemical and biological activities of the gamma-irradiated blended fibroin/aloe gel film. *ScienceAsia*, *48*, 278. https://doi.org/10.2306/scienceasia1513-1874.2022.048

Pierce, G. F. (2001). Inflammation in nonhealing diabetic wounds: the space-time continuum does matter. *The American journal of pathology*, *159*(2), 399-403.

Pu, H., Sun, Q., Tang, P., Zhao, L., Li, Q., Liu, Y., & Li, H. (2018). Characterization and antioxidant activity of the complexes of tertiary butylhydroquinone with β-cyclodextrin and its derivatives. *Food chemistry*, *260*, 183-192.

Raghow, R. (1994). The role of extracellular matrix in postinflammatory wound healing and fibrosis. *The FASEB journal*, *8*(11), 823-831.

Robson, M. C., Steed, D. L., & Franz, M. G. (2001). Wound healing: biologic features and approaches to maximize healing trajectories. *Current Problems in Surgery*, *38*(2), 72-140. https://doi.org/10.1067/msg.2001.111167

Roggin, K. K., Kim, J. C., Kurkchubasche, A. G., Papa, E. F., Vezeridis, A. M., & Tracy Jr, T. F. (2001). Macrophage phenotype during cholestatic injury and repair: the persistent inflammatory response. *Journal of pediatric surgery*, *36*(1), 220-228.

Roslev, P., & King, G. M. (1993). Application of a tetrazolium salt with a water-soluble formazan as an indicator of viability in respiring bacteria. *Appl Environ Microbiol*, *59*(9), 2891-2896. https://doi.org/10.1128/aem.59.9.2891-2896.1993

Schnider, S. L., & Kohn, R. (1981). Effects of age and diabetes mellitus on the solubility and nonenzymatic glucosylation of human skin collagen. *The Journal of clinical investigation*, *67*(6), 1630-1635.

Spanheimer, R. G., Umpierrez, G. E., & Stumpf, V. (1988). Decreased collagen production in diabetic rats. *Diabetes*, *37*(4), 371-376.

Su, D., Ding, S., Shi, W., Huang, X., & Jiang, L. (2019). Bombyx mori silk-based materials with implication in skin repair: Sericin versus regenerated silk fibroin. *Journal of Biomaterials Applications*, *34*(1), 36-46.

Tracy Jr, T. F., Dillon, P., Fox, E. S., Minnick, K., & Vogler, C. (1996). The inflammatory response in pediatric biliary disease: macrophage phenotype and distribution. *Journal of pediatric surgery*, *31*(1), 121-126.

Tziotzios, C., Profyris, C., & Sterling, J. (2012). Cutaneous scarring: Pathophysiology, molecular mechanisms, and scar reduction therapeutics Part II. Strategies to reduce scar formation after dermatologic procedures. *Journal of the American Academy of Dermatology*, *66*(1), 13-24; quiz 25-16. https://doi.org/10.1016/j.jaad.2011.08.035

Unger, R. E., Wolf, M., Peters, K., Motta, A., Migliaresi, C., & Kirkpatrick, C. J. (2004). Growth of human cells on a non-woven silk fibroin net: a potential for use in tissue engineering. *Biomaterials*, *25*(6), 1069-1075.

Van Klingeren, B., & Ten Ham, M. (1976). Antibacterial activity of Δ9-tetrahydrocannabinol and cannabidiol. *Antonie van Leeuwenhoek*, *42*(1), 9-12.

Wang, Y., Kim, H.-J., Vunjak-Novakovic, G., & Kaplan, D. L. (2006). Stem cell-based tissue engineering with silk biomaterials. *Biomaterials*, *27*(36), 6064-6082.

Werdin, F., Tennenhaus, M., Schaller, H. E., & Rennekampff, H. O. (2009). Evidence-based management strategies for treatment of chronic wounds. *Eplasty*, *9*, e19.

Worasakwutiphong, S., Termwattanaphakdee, T., Kamolhan, T., Phimnuan, P., Sittichokechaiwut, A., & Viyoch, J. (2021). Evaluation of the safety and healing potential of a fibroin-aloe gel film for the treatment of diabetic foot ulcers. *Journal of Wound Care*, *30*(12), 1020-1028. https://doi.org/10.12968/jowc.2021.30.12.1020

Wynn, T. A., & Barron, L. (2010). Macrophages: master regulators of inflammation and fibrosis. *Seminars in Liver Disease*, *30*(3), 245-257. https://doi.org/10.1055/s-0030-1255354